Research Article ISSN 2833-0390

International Journal of Research in Oncology

Conventional and Laser Driven Accelerator Technologies for Cancer Treatment

Scarlat F[1,2]*, Stancu E[2] and Scarisoreanu A[2]

[1]*Valahia University of Targoviste, Targoviste, Dambovita, Romania.*

[2]*National Institute for Laser, Plasma and Radiation Physics, Magurele, Ilfov, Romania.*

***Correspondence:**
Scarlat F, Valahia University of Targoviste, Targoviste, Dambovita, Romania.

Received: 12 Jul 2023; **Accepted:** 27 Aug 2023; **Published:** 05 Sep 2023

Citation: Scarlat F, Stancu E, Scarisoreanu A. Conventional and Laser Driven Accelerator Technologies for Cancer Treatment . Int J Res Oncol. 2023 2(3): 1-22.

ABSTRACT

Starting from the concept of technology (applied knowledge) defined as the crossing of two multitudes, science and associated technique, this paper provides an overview of the technology of charged particle accelerators (leptons and hadrons) for radiation therapy. High energy lepton beams, 4-25 MeV, refer to electrons and photons, and hadron beams to protons of 50 - 250 MeV and carbon ions of 100 - 450 MeV/u. Achieving clinical values for medical therapy is achieved using: the induced electric field for the electron acceleration (betatron), the microwave electric field for electrons (linac), the magnetic field for steering accelerated electrons on a metal target to obtain braking radiation (betatron, and linac), the high-frequency electric field for heavy particles (cyclotron and its variants), wake electric field generated by laser radiation in electron plasma and the electric field generated by laser radiation in a metallic target for protons and ions. Resonant acceleration (or energy transfer from the external acceleration field to the corpuscular radiation), on a rectilinear trajectory, occurs when the particle velocity is equal to the wave phase velocity associated with the electric field. Cyclic resonance, in a magnetic field perpendicular to the plane of the equilibrium orbit, occurs when the rotation frequency of the particle is equal to the frequency of the radio frequency electric voltage. Conversely, the transfer of energy from the particle to the wave, for example, Cerenkov radiation generated in a dielectric medium, occurs when the speed of the beam is greater than the speed of light in that medium. In turn, radiation sources (Cerenkov, Synchrotron, and Free Electron Laser) generated by ionizing particles can be used to accelerate charged particles. In addition to using the principle of resonance during acceleration, there are other principles to be fulfilled, such as, for example, weak focus, intense focus, transversal stability and longitudinal stability. Based on these principles, a large number of resonant cyclic accelerators have been developed, which differ from each other by one of the quantities that varies synchronously with the particle's energy. These quantities are the magnetic field, B(T), the radius of the orbit, ρ(m), and the frequency – f (MHz). In this way, we have: the betatron for electrons, 40 MeV, ρ = 0.25 m, 5 tons, the synchrotron for protons, 250 MeV, ρ = (6 - 9) m, and the synchrotron for heavy ions, 450 MeV/u, ρ = (18 – 25) m. All have constant radius and the field B(t) varies synchronously with the energy. For these, the variable size is f_{RF} - decreases in proton synchrotron, B(ρ) - varies in isochronous proton cyclotron, isochronous carbon ion cyclotron and in non-scaling FFAG of hadrons. The transition, from conventional magnets of 1.8 T, to superconducting magnets of (4-10) T, led to the reduction of the size and weight of the accelerators, resulting in the following: synchrocyclotron (250 MeV, 9T, 0.25 m, 20 tons), the proton isochronous cyclotron (250 MeV, 4 T, 3.1 m, 90 tons) and the isochronous cyclotron for protons and ions therapy (5400 MeV, 4.5/2.45 T, 6.6 m, 700 tons). The development of relativistic laser technology ($a_0 > 1$), allows the transition from conventional technology for electric fields, (1-50) MV/m in vacuum, to laser technology with fields of ~ 100 GV/m in plasma for electron acceleration (Bubble regime) and intensities of 10^{24} W / cm^2 for the acceleration of protons and ions (TNSA and RPA). The therapeutic energy of heavy particles determines the depth of penetration in tumors located at depths of (1-33) cm and the intensity of the beam (1 nA = 6.24 x 10^9 p/s in proton therapy and 0.1nA in carbon therapy) ensures the fractional absorbed dose value in tumor of 2 Gy in 1L. In summary, this paper presents the principles of obtaining therapeutic energies for the treatment of malignant tumors by the particle acceleration method and the body's response through the energy absorbed in tumor from the radiation, as energy imparted by the photon radiation or as energy lost by the charged particle, both based on the characteristic of the deeply absorbed dose, for each type of ionizing radiation.

Keywords
Radiotherapy Accelerator Technologies Betatron, Linac, Synchrocyclotron, Isochronous Cyclotron, Synchrotron, NS FFAG Accelerator, Laser Wake-Field accelerator, TNSA, RPA.

Introduction

The technologies of particle accelerators intended for use in radiotherapy are presented in this work. Accelerator technology, (applied knowledge), defined as the crossing of two multitudes, science and associated technique, integrates about 30 specialties (or top technologies). For example: vacuum technology (science and technology of vacuum), acceleration technology (science or physics and technique of accelerator), laser technology (science and technique of laser), and so on.

In the text of this work, the term "medical accelerator" or "accelerator" briefly represents "accelerator technology", which includes the family of component technologies, starting with the injector technology, passing through the radiation technology and ending with the beam modulation technology, passive or active, at the dimensions the target (tumors).

After the introduction, the second paragraph presents the principle of resonant acceleration of charged particles on rectilinear and circular trajectories, the types of medical accelerators, the energies provided by them in the beams and the irradiated environment, and the interaction coefficients. These interaction coefficients act as a conversion unit from the beam energy to the energy absorbed in the target, the absorbed dose, the fundamental quantity of radiation dosimetry, valid in all types of ionizing radiation, all materials and all energies.

The therapeutic systems with high-energy electron and photon beams, based on Betatron and Linac medical accelerators, are presented in the third chapter, as sources and characteristics of the radiation beams. The therapeutic systems with proton/carbon ion beams, having as sources the isochronous cyclotron, the proton synchrotron and the proton and carbon ion synchrotron, are presented in chapter four.

New technologies based on superconductingmagnets, the synchrocyclotron for protons as well as the isochronous cyclotron and non-scaling FFAG accelerator, for providing both types of beams, protons and ions, are the subject of chapter five.

New laser-driven acceleration technologies are mentioned in chapter six. They use the ponderomotive force of the propagation of the relativistic laser pulse through plasma, to create a nonlinear plasma wave associated with a wake field of electron acceleration, the "bubble" method. Also, the acceleration of protons and ions through the **methods:** Target Normal Sheath Acceleration (TNSA) and Radiation Pressure Radiation (RPA) with relativistic radiation intensities are mentioned in the paper.

Medical accelerator for clinical therapy

As the science of the electron (JJ Thompson 1897), the existence of the proton (E. Rutherford, 1919) and the magnetic field technique (Oersted, 1900) were known, some technologies (or methods and associated devices) were developed, as follows: the acceleration of electrons in the induced electric field patented by Slepian (1921), linear acceleration of electrons, experimented by Wideroe (1928), acceleration of heavy particles (protons) patented by Lorentz (1929), model cyclotron built by Livingston (1931) and betatron built by Kerst (1940). Starting from these patents (or technologies) as well as other discovered principles, the first applications in radiotherapy were: the Betatron (1949), the Linacul (1953 - 1954) and the Cyclotron (Tobias 1955, Lawrence Brookhaven Livermore), [1,2].

Principles of charged particle acceleration.

The simplest model of a charged particle acceleration system is presented schematically in Figure 1.

INJECTOR → ACCELERATOR → RADIATION

Figure 1: Simple system for accelerating charged particles.

The first component, the injector, which in turn can be an accelerator, is the source of generating charged particles that must be accelerated (electrons, protons, and heavy particles).

The second component is the acceleration structure for the standard injector or a high-energy accelerator, when the injector is a low-energy accelerator. This also contains the extractor. The kinetic energy field gain (T) of the particle with electric charge q = e at the level of the extraction window is given by the force (F), the longitudinal electric $E_{\parallel}$ or voltage U, equation (1)

$$T = \int \vec{F} \cdot d\vec{s} = e \cdot \int E_{II} \cdot ds = e \cdot U. \quad (1)$$

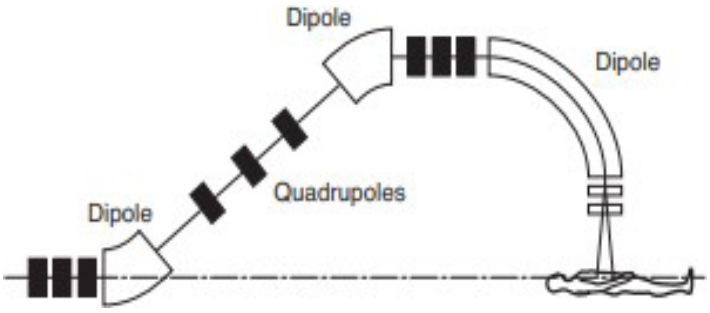

Figure 2: Gantry Downstream scanning system [3].

The third component between the extraction window from the accelerator and the patient entrance gate is the gantry with

upstream or downstream magnetic scanning for the radiation beam formed or modulated to the size of the tumor, and the treatment table, sketched in Figure 2 [3].

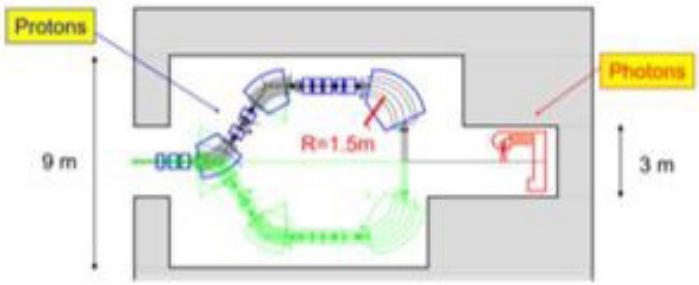

Figure 3: Proton Gantry for protons, Bρ < 2.4 Tm, and photons [4].

The complexity of a medical accelerator intended for radiotherapy, with hadrons or leptons, is shown in Figure 3 [4].

The resonant acceleration of particles on a rectilinear trajectory is produced by the interaction between the particle and a high-frequency electric field when the particle's speed is lower than or equal to the speed of the slow acceleration wave.

The resonant acceleration on a circular trajectory occurs at the equality between the frequency of the RF voltage in the resonant electric cavity, ω_{RF}, and the recirculation frequency of the accelerated particle ω_{rev}, **[5]**.

Particle acceleration occurs in vacuum, gases, or plasmas. It can be driven conventionally in radiofrequency fields, or by a laser in relativistic mode [**6**].

Types of Medical Accelerators

Leaving aside the linear accelerators, the cyclic acceleration of the particles up to a kinetic energy higher than 1-1.5% of the rest energy, requires that in the condition of resonance

$$\omega_{rev} \equiv \frac{qB}{m} = \omega_{RF}\ \omega_{rev} \qquad (2)$$

where one of the quantities ω or B (or both) should be variable in time to follow the mass increase with the Lorentz factor, $m = m_0\gamma$.

Based on the theory of phase stability (or self-phasing), a large number of resonant cyclic accelerators have been developed, which differ from each other by the size that varies during acceleration to maintain resonance (longitudinal motion - synchrotron oscillations) and by the way it is ensured orbital stability (transverse motion – betatron oscillations), [7]. Some types of medical accelerators are shown in Figure 4.

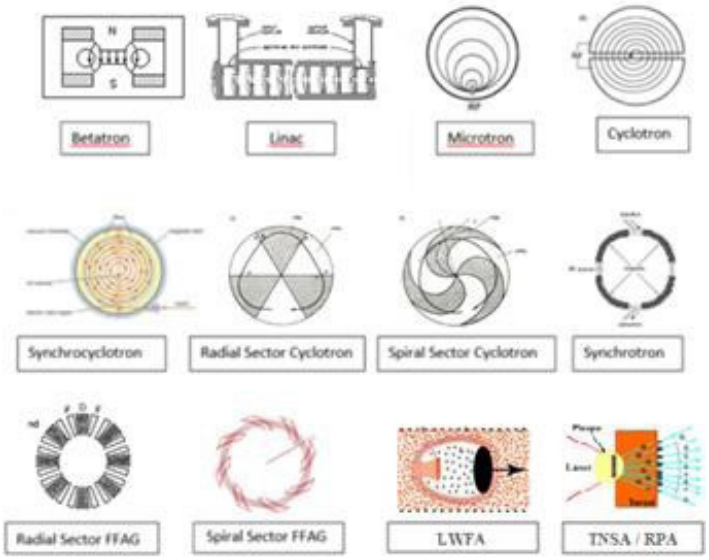

Figure 4: Acceleration technologies discussed in this paper: a) Betatron [B(t), ; b) Linac (B=0, f=const); c) Microtron ρ = variable); d) Classic Cyclotron (ρ increases with energy); e) Synchrocyclotron or phasotron (f = varies, ρ increase with energy); f) Radial Sector Cyclotron (B varies, ρ = increases with energy); g) Isochronous Cyclotron Spiral Sector (B=varies, ρ = increases with energy; h) Synchrotron of protons or Synchro-phasotron (B=varies, f = varies, ; i) Radial Sector Scaling FFAG or Ring Phasotron (B varies with radius , f = variable, ρ = increases with energy,); j) Radial Sector Non-Scaling FFAG (B varies with radius, ρ = increases with energy); k) Spiral Sector FFAG (B varies with radius; f and ρ increases with energy, and l) LWFA – Laser wake field accelerator for electrons, TNSA - Target Normal Sheath Acceleration and RPA - Radiation Pressure Acceleration for protons and ions.

Energy supplied by accelerated beams

In the macroscopic domain, the radiation field, a region of vacuum or substance permeated by radiation, operates with average values to be described by continuous functions of coordinates and time. These refer to radiometric and macroscopic dosimetric quantities used in radiological protection [8,9].

To define them, a volume (V) is chosen from the irradiated environment, which surrounds the mass, m = ρV. This is high enough to neglect the statistical fluctuations of the characteristic quantities of the radiation field, and at the same time low enough, so that the values of these average quantities can be considered "punctual" and "instantaneous".

The charged particles, with speed v = β.c, c = speed of light, are characterized by the total energy $\mathcal{E} = \gamma\mathcal{E}_0$, consisting of the rest energy $\mathcal{E}_0 = m_o c^2$, and the kinetic energy $T = mv^2/2$. Using the invariant, $\gamma^2 - \beta^2\gamma^2 = 1$, we obtain the relationship between energy and impulse.

$$\mathcal{E}^2 - p^2c^2 = \mathcal{E}_0^2, \qquad (3)$$

where $p = m_0 v$ is the non-relativistic impulse (or moment); pc = βE, is the relativistic kinetic energy and c = 299, 792, 458 m/s (≈ 2,998 x 10^{88} m/s) is the light velocity in vacuum.

The particle gains kinetic energy through the associated impulse with the total energy, p, which in the case of the existence of a magnetic field is described by the relation:

$$p = qB\rho, \tag{4}$$

where B is the magnetic field, ρ is the radius of curvature, and their product, B·ρ, is called the magnetic rigidity of the beam,

$$B \cdot \rho = \frac{\sqrt{T^2+2T\mathcal{E}_0}}{300Q} \quad , \tag{5}$$

where q = e·Q and Q is the charge ionization number of the particle. The rest energy, $\mathcal{E}_0$, and the kinetic energy, T, are expressed in MeV and the rigidity B·ρ in T·m.

The quanta of the electromagnetic field are photons, particles with zero rest mass, without electric charge, which propagate with the speed of light in a vacuum. The average power per unit area transported by an electromagnetic wave is called "intensity",

$$I(W/cm^2) \equiv \langle \vec{S} \rangle = \langle \frac{1}{\mu_0} \vec{E} \times \vec{B} \rangle = \epsilon_0 c \frac{E_0^2}{2} \vec{z}, \tag{6}$$

where $_0$ is the electric rigidity, E_0 is the magnitude of the electric field, and $z^{\rightarrow}$ is the direction of Poynting vector, $S^{\rightarrow}$.

Energy and impulse (or momentum) of the electromagnetic waves stored in volume V (m^3) are defined as follows:

$$\mathcal{E}(J) = \frac{I}{c} V; \qquad p(J \cdot s/m) = \frac{1}{c^2} V. \tag{7}$$

For an intense laser pulse ($a_0 \equiv eE/\omega m_0 c > 1$), the radiation intensity I, given by the pulse energy E per beam cross-section A and pulse duration τ, is

$$I(W/m^2) \equiv \frac{\mathcal{E}}{A\tau} = 1{,}38 \times 10^{18} a_0^2/\lambda_0^2(\mu m). \tag{8}$$

The ponderomotive force (or nonlinear force) responsible for the drift movement of the particle, is given by

$$F_p(N) \equiv -\nabla \Phi_p = -\frac{e^2}{4m_e\omega_L^2} \nabla \langle E^2 \rangle, \tag{9}$$

where Φ_p is the ponderomotive potential, $\nabla\langle E^2\rangle$ is the cycle averaged gradient in the field seen by the electron, ω_L is the laser frequency, and m_e is the electron rest mass. Details in [10].

Energy in interaction processes of particles

Energy imparted by ionizing radiation to the matter

The energy deposit ε_i (stochastic quantity) is the energy deposited in a single interaction i: $\epsilon_i = \epsilon_{in} - \epsilon_{out} + Q$, where the entry and exit from the volume are denoted by in and out, and Q is the change in the rest energies of the nucleus and of all particles involved in the interaction: (Q > 0 for m → γ and Q < 0 for γ → m), [1].

The energy imparted, $\boldsymbol{\epsilon}$, to the matter in a given volume, is the sum of all energy deposits in the volume, thus $\boldsymbol{\epsilon} = \sum_i \boldsymbol{\epsilon}_i$. Conform ICRU 1980, the energy imparted is $\epsilon = R_{in} - R_{out} + \sum_n Q_n$, where R = ∑ T, (the sum of the kinetic or quantum energies of ionizing particles) is called radiant energy.

The mean energy imparted, $\bar{\epsilon}$ (J), is given bu the equation $\bar{\epsilon} = \bar{R}_{in} - \bar{R}_{out} + \overline{\sum Q}$, where the bars indicate the expected values. The absorbed dose, D, is defined as (ICRU 1980),

$$D = \lim_{m \to 0} \frac{\bar{\varepsilon}}{m} = \lim_{V \to 0} \frac{1}{\rho} \frac{\bar{\varepsilon}}{V}, \tag{10}$$

where m is the mass contained in an infinitesimal volume V.

The expectation value of the energy imparted ϵ^- is determined using the Poynting theorem. The net transport $\bar{R}_{in}$ - $\bar{R}_{out}$ of the radiant energy through the surface element dA in the direction -$dA^{\rightarrow}$ i.e., into the volume, is given by the scalar product -$\vec{\Psi}_c \cdot dA^{\rightarrow}$. Result,

$$\bar{\epsilon} = \int_V D\rho dV = \iiint div\, \vec{\Psi} dV + \overline{\Sigma Q}). \tag{11}$$

Correction of the balance with the term $\overline{\Sigma Q} \equiv Y$ it is important only in the case of high energies, with positive and negative variations of rest energies - respectively masses - based on the Einstein relation from the theory of relativity.

The fundamental equation of radiation dosimetry for Y= Y_c = 0, can be written as follows **[11],**

$$D = -\frac{1}{\rho} div\, \vec{\Psi} = -\frac{1}{\rho} div\, \vec{\Psi}_u - \frac{1}{\rho} div\, \vec{\Psi}_c - \frac{1}{\rho} div\, \vec{\Psi}_{c,s}, \tag{12}$$

where the radiation field was divided into different components: the uncharged ionizing particle field ($\vec{\Psi}_u$), the charged primary ionizing particle field ($\vec{\Psi}_c$), and the charged secondary ionizing particle field ($\vec{\Psi}_{c,s}$). The unit of absorbed dose is joule per kilogram (J/kg), or gray (1 Gy = 1 J/kg = 6.24 x 10^9 MeV/g).

Energy transferred by photons.

Photons themselves do not transfer energy. Upon irradiation with a photon beam, the dose absorbed in the volume V is

$$D = -\frac{1}{\rho} div \vec{\Psi}_u = K - B = K_{col}, \tag{13}$$

where K = K_{col} + K_{rad} is the total kerma composed of collision kerma K_{col} and radiation kerma K_{rad} , B = dE_B/dm, is the energy that leaves the volume V and K_{col} represents the energy remaining in the volume V. For monoenergetic photons, the total kerma K at a point in a medium is K≡ dE_{tr}/dm. The unit of kerma is joule per kilogram (J/kg) or gray (Gy), [1].

Using the photon energy fluence rate, $\dot{\Psi}_u$ (J/cm².s), the calculation relation for the quantity kerma rate is obtained**,** *K*, [12].

$$\dot{K} \equiv \left(\frac{1}{\rho}\right) \cdot \frac{d\Psi_u}{dx} = \frac{\mu_{tr}}{\rho} \dot{\Psi}_u, \tag{14}$$

where (μ_{tr}/ρ) in units (m^2/kg), is the linear energy-mass transfer coefficient, which acts as a conversion unit from photon energy fluence rate to total kerma. It is defined by the expression,

$$\frac{\mu_{tr}}{\rho} = \frac{1}{\rho}\left[\tau\left(1-\frac{\delta}{h\nu}\right)+\sigma\frac{\overline{E_c}}{h\nu}+K\left(1-\frac{2m_0c^2}{h\nu}\right)\right]. \quad (15)$$

In relation (15) we have: the quantity $\mu/\rho = (\sigma + \tau + \kappa)/\rho$ is the total linear attenuation coefficient, that is, the sum of the partial coefficients of the three major interactions (effect: Compton - σ, photoelectric - τ and pair production – κ) and the quantities δ, $\overline{Ec}$, $2m_0c^2$ represent, respectively, the average energy of the characteristic radiation that appears in the photoelectric effect, the average Compton scattering energy and the annihilation energy that appears in the pair production process (e-, e+).

In the case of electronic balance (CPE), div $\vec{\Psi}_c = 0$ and D = K – B. In the additional hypothesis that the energy of the primary photons and that of the secondary electrons is not too high, B = 0, and K_{rad} = 0 because photons do not transfer energy. The absorbed dose produced during photon irradiation is equal to collision kerma,

$$D = K_{col} = \frac{\mu_{ab}}{\rho}\Psi_u\,, \quad (16)$$

where μ_{ab} the energy-mass absorption coefficient is

$$\frac{\mu_{ab}}{\rho} = \frac{1}{\rho}\left[\tau\left(1-\frac{\delta}{h\nu}\right)+\sigma\frac{\bar{E}_c}{h\nu}+\kappa\left(1-\frac{2m_0c^2}{h\nu}\right)\right](1-g)\,, \quad (17)$$

with g = fraction of energy lost by secondary electrons in bremsstrahlung processes and (μ_{ab}/ρ) is the mass energy absorbed coefficient.

Energy lost by ionizing charged particles.

Charged particles (electrons, protons, etc.) release energy to the environment. When a beam of charged particles irradiating an environment, the absorbed dose is related to the electron fluence, Φ_e,

$$D_m = -\frac{1}{\rho}\,\mathrm{div}\,\vec{\Psi}_c = \Phi_e\left(\frac{S_{el}}{\rho}\right)_m = \Phi_e\frac{L_\infty}{\rho}\,, \quad (18)$$

where the interaction coefficient, $S_{el}/\rho dl \equiv (S_{col}/\rho dl) = (S/\rho dl) - (S_{rad}/\rho dl)$, is the mass electronic stopping power of a specified material of density ρ for charged particles of energy E, and L_∞ is the corresponding unrestricted linear energy transfer.

The Bragg – Gray (B-G) cavity theory was the first cavity theory developed to provide a relation between the absorbed dose in a dosimeter and the absorbed dose in the medium containing the dosimeter.

Using abbreviated notations, the dose in the cavity, $D_c = \Phi_e(S_{el}/\rho)$, identical fluency Φe, and the Bragg-Gray conditions [1] fulfilled, the dose in the medium without a cavity is

$$D_m = D_c\,.\left(\frac{S}{\rho}\right)_m/\left(\frac{S}{\rho}\right)_c\,. \quad (19)$$

If it has instead of the interaction coefficient L_∞/ρ is used the linear energy transfer, LET, or the restricted linear electronic stopping power, L_Δ, of a material, for charged particles of a given type and energy, the quotient of dE_Δ by dl, where dE_Δ is the mean energy lost by the charged particles due to electronic interactions in traversing a distance dl, minus the mean sum of the kinetic energies in excess of Δ of all the electrons released by the charged particles, thus

$$\frac{L_\Delta}{\rho} \equiv \frac{dE_\Delta}{\rho dl} = \frac{S_{el}}{\rho} - \frac{dE_{k,\Delta}}{\rho dl}\,. \quad (20)$$

In this case, the absorbed dose is given by the relationship:

$$D\,(Gy) \equiv C_\Delta = 1.6\cdot10^{-9}\cdot\frac{1}{\rho}\frac{dE_\Delta}{d\ell}\left[\frac{keV}{\mu m}\,\frac{cm^3}{g}\right)\cdot\ \Phi_e[cm^{-2}]\,. \quad (21)$$

Aceasta doza coincide cu conceptul, 'restricted cema", noted with C_Δ, $C_\Delta \equiv {}_\Delta/\rho)\,\Phi_e$, (A. M. Kellerer et al., 1992).

The general calculation formula for the absorbed dose, based on the formalism $N_{D,w}$ - IAEA – TRS 398, in the reference point D w,(z-ref) at any user quality Q (photons, electrons, protons, heavier particles), is given by the formula (22),

$$D_{w,Q} = M_Q \text{ x } N_{D,W,Q0} \text{ x } k_{Q,Q0}\,, \quad (22)$$

where M_Q = Instrument reading at users beam quality Q, corrected for all influence quantities other than beam quality, $N_{D,W,Q0}$ = Absorbed dose to water calibration coefficient for calibration beam quality Q_0 (= Co-60) , $k_{Q,Q0}$ = Beam quality factor to correct for effects of differences between calibration beam quality Q_0 and user beam quality Q, [13].

High energy photon/electron beam therapeutical systems

High energy photon beams for external radiotherapy are generated by electron accelerators: betatron, linear accelerator, synchrotron, microtron, Vaan de Graff and cyclotron. To these we can add the gamma radioactive sources Co-60 of 1.33 MeV (100%), 1.17 MeV (100%) and the source of Cs-137 of 0.66 MeV (85% of disintegrations) [14].

Clinical photon beams (or braking radiation) are obtained by the interaction of electrons accelerated to kinetic energies (2 - 45) MeV, with a metal target with a high atomic number Z, such as: tantalum, platinum. gold etc.

The main types of accelerators and sources used in external therapy are presented in Table 1 [15].

Table 1: IAEA Worldwide Register of Teletherapy Units.

Linear Accelerators		Betatrons	60-Cobalt and 137-Cesium units	
Year	**1967**	**1967**	**1967**	**1967/1962**
Europe	33	88	604	1.2
North America	-	288	651	1.3
Japan	8	16	328	1.4
Asia less Japan	3	3	83	3.3
Central and South America	0	1	12	2.3
Africa	0	0	13	1.3
Australia and New Zeeland	7	1	16	1.9
Total	105	137	1816	1.4

Table 1 shows that, in 1967, about 105 medical linear accelerators, 137 medical betatrons, which provided electron and photon beams (or braking radiation) and 1816 Co-60 sources, which provided radiation beams, were used in external radiotherapy gamma with the equilibrium dose constant, Δ (gmGy/MBq-hr) = 767 for 1.33 MeV & 674 for 1.17 MeV, and Γ (R-cm^2/hr-MBq) = 0.36 for Pb HVL = 1 cm. Similarly, Cesium137 sources were used with β-rays of 0.514 MeV (95%) and γrays of 0.661 MeV (85%), and the constant Γ (R-cm^2/hr-MBq) = 0.089 R/hr; for Pb HVL= 0.5 cm.

Medical accelerators of electrons/photons

The first accelerator used in therapy was the Betatron in 1949 **[16]**, followed by the Linear Accelerator, after the discovery of microwave sources (magnetron-1941 and clystron-1948), in 1953-1954 **[17]** and the proton cyclotron in 1954. The betatron was patented in 1921 by Slepian. Wideroe established the stability condition for the equilibrium orbit (1928), Steenbek – the weak focusing principle (1934), and Kerst built the first betatron in 1940.

The working principle of the betatron is based on the law of electromagnetic induction discovered by Faraday (1831).

According to this law, the time-varying magnetic field, B(ρ_0, t), with the standard frequency of 50-60 Hz, induces a circular variable electric field E(t), at the radius of the equilibrium orbit ρ_0. Voltage V, used to accelerate electrons, is given by the induction Faraday law, so:

$$V = \oint E\, d\rho = \int_S rot\vec{E}\, d\vec{S} = -\frac{d}{dt}\int_S \vec{B}\, d\vec{S} = \pi \rho_0^2 \frac{d\bar{B}}{dt} \quad (23)$$

The gantry containing the betatron, weighing 5 tons, at E = 40 MeV, is presented in figure 5 **[18].**

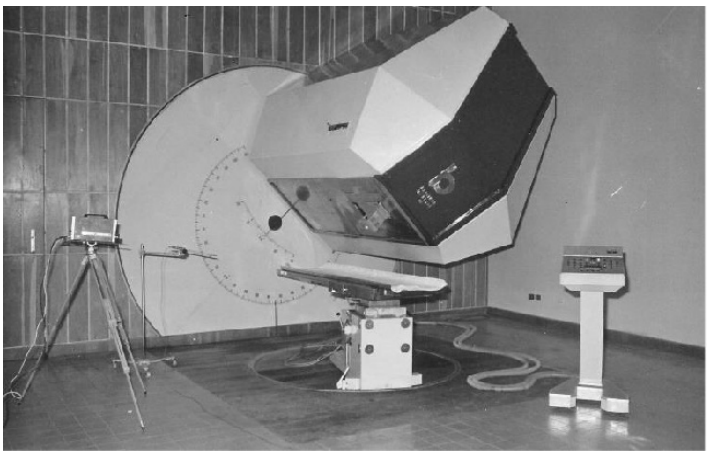

Figure 5: 40 MeV IFA Medical Betatron.

The kinetic energy of the accelerated electrons (T = $\mathcal{E}$ - $\mathcal{E}_0$) in the betatron, which determines the range of the charged particles in the irradiated medium, is calculated using the general formula, obtained from the Lorentz invariant

$$T = \sqrt{(pc)^2 + (m_0c^2)^2} - m_0c^2 , \quad (24)$$

where $\mathcal{E}_0^2 = m_0c^2$ is the rest energy of the electron (m_0 = 0.511 MeV/c^2), pc = the relativistic kinetic energy of the electron,

$$pc\ (MeV) = = 299.8 \frac{MeV}{(V/m).s} E(V/m).T_{acc}(s) , \quad (25)$$

in the case of movement in an electric field, E (V/m), in the acceleration time, T_{acc} (seconds), or.

$$pc\ (MeV) = = 299.8 \frac{MeV}{Tm)^2} B.\rho\ (Tm) . \quad (26)$$

in the case of movement in a magnetic field, B(T) at radius ρ (m).

The equality of relations (25) and (26) helps to determine the value of the induced electric field E(V/m), for the electron acceleration in betatron. For a betatron with relativistic kinetic energy, T ≡ 40 MeV ≈ pc, because 40 MeV >> 0.511 MeV, results: E = 20 V/m. Other values for quik calculation are: the magnetic rigidity, B·ρ_0 = 0.10 Tm, B (ρ_0) = 0.4 T and ρ_o = 0.25 m and T_{acc} = 5 x 10^{-3} second.

Companies that built medical betatrons, are: Aliss Chalmers (22 MeV), Siemens (42 MeV), Brown Bowery (45 MeV), Mitubisi (25 MeV). The weight of the electromagnet of a betatron being relatively high, for example 5 tons at 40 MeV and the current of accelerated electrons of low value, a few μA, led to the replacement of the betatron technology, based on an induced electric field, with the linac technology, based on traveling electromagnetic waves or stationary, which has much less weight and a current of accelerated electrons of relatively high values, Figure 6, [19].

The operating principle of the linear accelerator is based on the resonance phenomenon, which occurs when the particle speed is equal to the phase speed of the slow RF wave, due to the "irises" introduced in the acceleration structure.

Figure 6: 10 MeV Electron Linac.

The electron beam passes once through a large number of acceleration cavities determined by the programmed energy.

Energy gained after n acceleration gaps:

$$T_n = n\, q\, U_0 \sin \varphi_s\,, \qquad (27)$$

where n number of acceleration cavities, q charge of the particle, U_0 peak voltage of the RF system and Φ_S synchronous phase of the particle.

The medical LINear ACcelerator (LINAC) is a device that accelerates electrons on a linear trajectory from the injection energy of 50-100 kV to the therapeutic energy between 4 and 25 MeV, using a longitudinal electric field of radiofrequency (2856 MHz - S band).

For 3 MeV IFA linac with kinetic energy T = 3 MeV, a quick calculation with relation (25) determines the value of the relativistic kinetic energy pc = 3.47 MeV. The application of relation (25), to determine the value of the electric acceleration field E(V/m), requires the determination of the acceleration time on the two sections: non-relativistic (β = 75 c) and relativistic (β = 0.95 c). At the lengths (0.22 m; 1.03m) correspond the acceleration times ((0.1 x10^{-8}s; 0.35 x 10^{-8}s) and a total time t = 0.45 x 10^{-8}s. At these values, the acceleration electric field is E = 2.57 MV/m, over 10^5 times the electric field from betatron.

Compared to the betatron, which allows obtaining clinical energies between 10 and 45 MeV, the linac provides only one programmed energy per X Rays or electron operating mode.

Clinical high energy photon beam systems

Photons with energies in the range of 4-25 MeV are generated by the betatron and the linac. The energy of the photons at the values fixed for the treatment in the range above is controlled electronically in the case of the betatron and has a fixed value in the linac Transversal beam modulation is obtained through beam spread and beam absorption, Figure 7, **[20].**

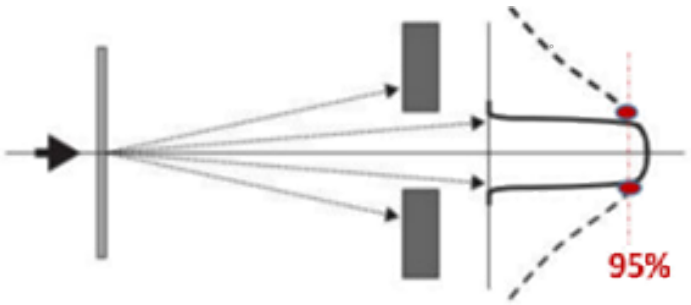

Figure 7: Distribution of the photon beam at the window of extraction from the accelerator (Betatron or Linac).

In order to be used in the treatment of malignant tumors, the photon beam is processed in order to obtain irradiation fields, between (4 x 4) cm^2 and (40 x 40) cm^2, at the source-skin distance, SSD = 1 m**.** The transformation of the Gaussian curve into a rectangular shape is produced with the help of a special channel for the formation of the photon beam, shown in Figure 8, [21].

The beam of accelerated electrons in the linear accelerator is oriented in the forming channel with the help of an alpha magnet. At the electron-target interaction, bremsstrahlung radiation with a Gaussian spectrum is produced. Using this forming channel, the distribution of the dose absorbed in depth is obtained, on the axis of the radiation beam with the energy of 10 MeV, shown in Figure 9 [21].

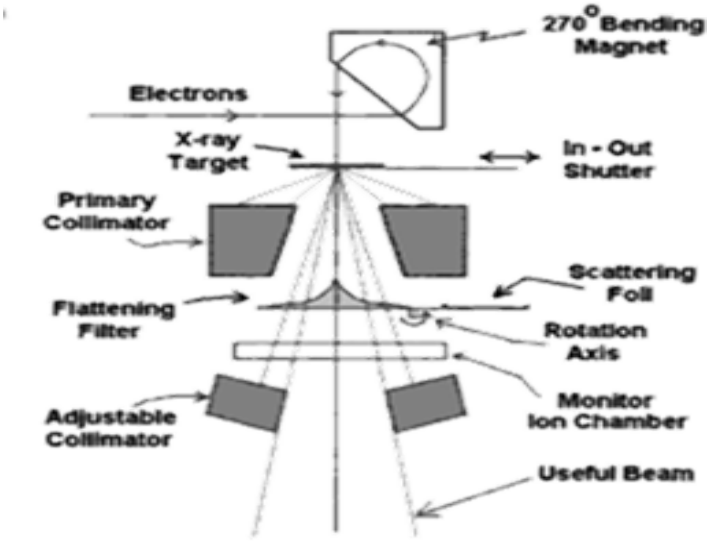

Figure 8: X-ray beam forming a channel in Linac.

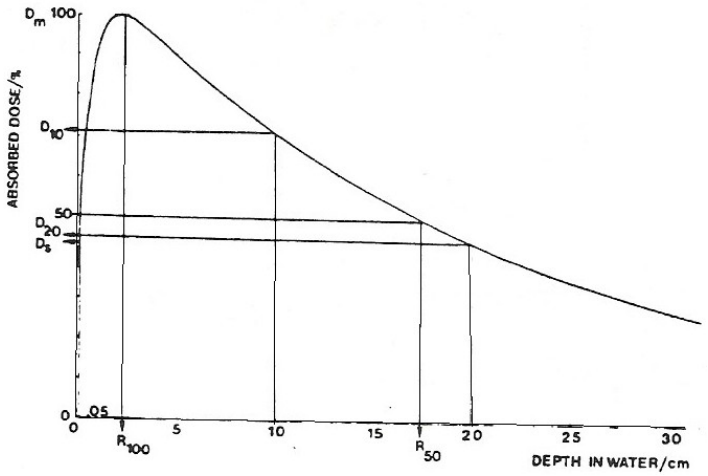

Figure 9: Central axis depth dose curve for a typical 10 MeV photon beam.

From this distribution, the necessary parameters are obtained for the development of the treatment plan in the photon radiation field, as follows: D_m is the maximum absorbed dose, D_s the surface dose measured at 0.05 cm depth, R_{100} the depth of dose maximum and R_{50} the half value depth.

The quality factor of the high-energy photon beam, $TPR_{20,10}$, is determined by the ratio of absorbed doses at depths of 20 cm and 10 cm in a water phantom. The source-to-camera distance (SCD) is kept constant. Also, the absorbed dose to the skin, obtained from the distributions of the absorbed dose in depth for energies

between 4 MeV and 25 MeV, is important in external radiotherapy, Figure 10.

The percentage depth dates for various photon beams in a water phantom with a field size of 10 x 10 cm^2, an SSD of 100 cm and two depths: 5 cm and 10 cm, are presented in Table 2.

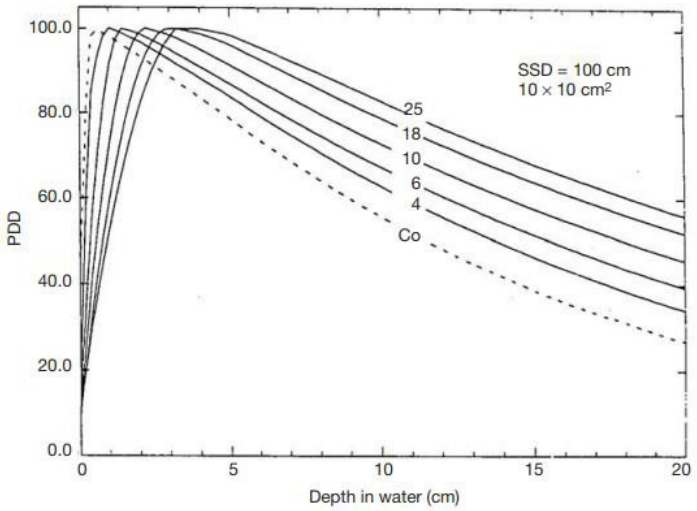

Figure 10: PDD curves in water for a 10 × 10 cm^2 field at an SSD of 100 cm for various energy photon beams ranging from ^{60}Co γ rays to 25 MeV X rays [22].

Table 2: Percentage depth dates for z_{max}, 5 and 10 cm.

	Co-60	4 MV	6 MV	10 MV	18 MV	25 MV
zmax	0.5	1,0	1.5	2.5	3.5	5,0
5 cm	80	84	86	72	97	98
10 cm	59	65	67	94	80	82
TPR20,10	0.519	0.581	0.626	0.688	0.745	0.768

The reference conditions for determining the absorbed dose in water for high-energy photon beams are defined in IAEA TRS 398, [13].

The main parameters for the energies between 1.25 MeV and 45 MeV, starting with the Co-60 source and ending with the data from a 45 MeV medical betatron, are presented in Table 3, (H. Svenson Course).

Table 3: Photon beam characteristics generated by Co-60, and electron accelerators.

Accelerator / Energy (MeV)	D10 /D20	Ds /D10	R100 cm	R50 cm	Ds / Dm	Reference
^{60}Co / 1.25	1.97	1.95	0.5	12.1	-	HPA(1972)
Van de Graaff / 2	2.18	2.12	0.4	11.1	-	HPA(1972)
Van de Graaff/ 4	1.84	1.82	1.0	13.7	-	HPA(1972)
Linac / 4	1.88	1.87	1.0	13.3	-	Castro et coll. (1972)
Linac / 6	1.73	1.73	1.8	15.4	0.43	HPA(1972)
Linac / 8	1.64	1.64	2.2	17.0	0.34	HPA (1972)
Linac / 10	1.60	1.60	2.3	17.8	0.18	Connor et coll (1976)
Microtron / 10	1.60	1.60	2.1	17.5	0.37	Svensson, H., Course
Linac / 15	1.53	1.52	2.7	20.1	0.27	HPA(1972)
Linac / 16	1.53	1.53	2.6	19.9	0.64	IAEA (1976)
Linac / 18	1.50	1.49	2.9	20.9	0.43	Noel et coll (1976)
Betatron / 20	1.50	1.48	3.3	21.6	0.53	HPA(1972)
Microton / 21	1.53	1.53	3.0	20.3	0.29	Svensson, H.,Course
Betatron / 24	1.45	1.42	3.9	23.8	0.17	HPA(1972)
Linac / 25	1.50	1.47	3.7	22.1	0.35	Podgorsak et coll 1974
Linac / 25	1.46	1.43	3.7	23.3	0.30	Tapley 10973
Betatron / 25	1.45	1.38	4.7	24.9	0.22	Podgorsak et coll 1974
Synchrotron / 30	1.47	1.38	4.7	24.3	0.45	Mitchell et coll 1953
Betatron / 31	1.42	1.36	4.7	25.9	-	HPA(1972)
Betatron / 35	1.39	1.33	4.9	27.4	-	NACP(1972)
Betatron / 35	1.43	1.40	4.0	24.9	0.30	NACP(1972)
Betatron / 42	1.43	1.36	4.2	25.6	0.64	NACP(1972)
Betatron / 45	1.42	1.35	4.4	26.1	0.60	NACP(1972)

Table 3 includes parameters for medical Van de Graaff accelerators of 2 MeV and 4 MeV, linacs of 4, 6, 8, 10, 15, 16, 18, and 25 MeV, microtron of 10 MeV and 21 MeV, synchrotron of 30 MeV, and betatrons of 20, 24, 25, 31, 35, 42, and 45 MeV. Column 5 of table 3 shows the values of the depth R_{100} (cm) for the value of the maximum dose D_m =100%, between 5 mm for the average energy of 1.25 MeV, 44 mm for the energy of 45 MeV (Betatron) and 45 mm (linac 25 MeV). Also, the ratio between the dose to the skin (entering the body) D_s, which produces erythema, and the maximum dose D_m, varies between 0.43 at 6 MeV and 0.64 at 42 MeV. For the energy of 1.25 MeV provided by Co-60, which has the maximum dose at a depth of 0.5 cm, the dose at the surface is 95%.

The reference conditions for determining the absorbed dose in water for high energy photon beams are defined in IAEA TRS 398.

Photon radiation has two main problems in the treatment of deep tumors: (1) they deposit unwanted doses in critical organs close to the target volume (see Figure 11) and (2) they cannot cure so-called "radioresistant" tumors that are less sensitive to radiation than the surrounding normal tissues.

The analysis in Figure 11, which shows an irradiation with photon beams and next to it an irradiation with proton beams, concludes the advantages of the treatment with hadron beams.

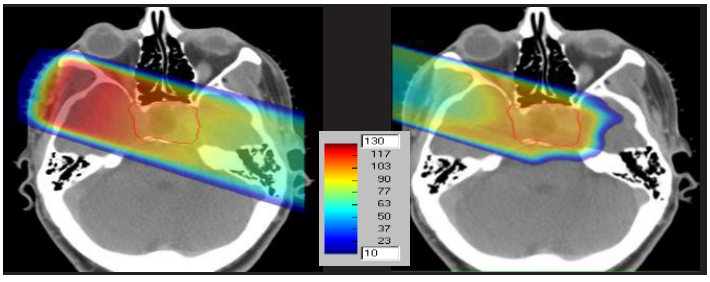

Figure 11: The advantages of hadron therapy [23].

To focus a higher dose of X-rays on the tumor, while reducing the radiation exposure of the surrounding normal tissues, it is used the Intensity- Modulation Radiation Therapy (IMRT) Method. Details in ICRU83, [24,25].

IMRT is an advanced mode of high-precision radiation therapy that uses computer-controlled X-ray accelerators to deliver precise doses of radiation to a malignant tumor or specific areas within the tumor. The radiation dose is designed to conform to the three-dimensional (3-D) shape of the tumor by modulating or controlling the intensity of the external radiation beam. IMRT tries to achieve more optimal absorbed dose distributions by varying the beam intensity (or energy fluence rate) within each incident beam.

Clinical high-energy electron beam systems

The medical linear accelerator produces electron beams with discrete energies in the range from 4 to 25 MeV. The electron beams at the exit window of the accelerator have the spectrum shown in Figure 12.

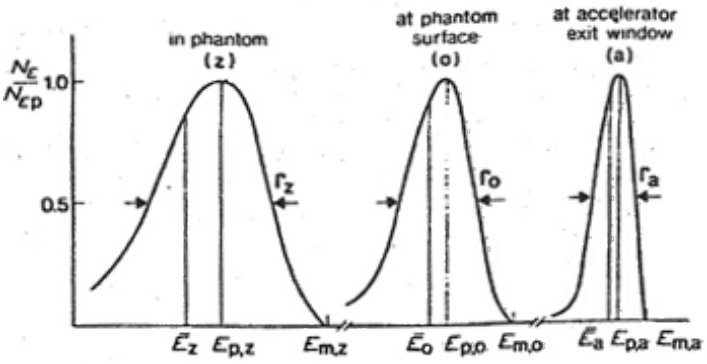

Figure 12: The distribution of electron beams extracted from Linac and Betatron [26].

The spectrum is presented in three situations: at accelerator exit window (a), at the phantom surface (0) and at the phantom depth (z), for three values of the average energy; maximum energy (E_m), the most probable energy (E_p) and the mean energy ($\bar{E}_0$). To transform the peak distribution into a uniform distribution at the input gate of the phantom, an electron beam shaping channel is used to the one shown in Figure 8 for photons, which does not contain the scattering folie.

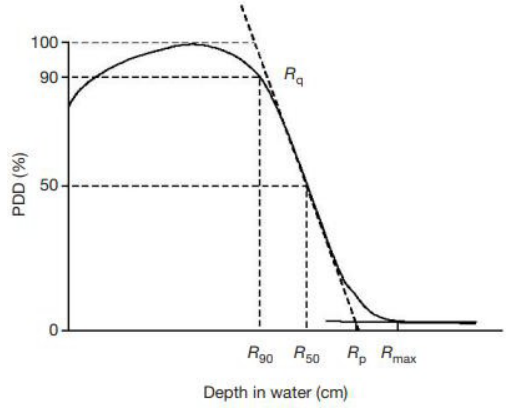

Figure 13: Depth vs. absorbed - dose with definitions of all the parameters used in the text.

The central axis depth dose curve of a typical clinical electron beam with energies between 4 MeV and 25 MeV, homogenized, is presented in Figure 13.

The response curve to the irradiation with a high-energy electron beam, has marked the main characteristics of the dose distribution in the biological tissue during electron irradiation. Among these, we mention: $R_{max} = R_{100}$ maximum range for z maxim, Rp = practical range, R_{90} = therapeutic range, R_{85} = therapeutic range, R_{50} = depth and Rq = the gradient depth in R_{50} at D_{50} corresponding to the maximum dose, $D_{100.}$

Regarding the dose values at the surface of the phantom, they are presented in Table 4.

Table 4: Electron beam depth dose parameters.

Energy (MeV)	Surface Dose (%)	R90 (cm)	R80 (cm)	R50 (cm)	Rp (cm)	$\bar{E}0$ (MeV)
6	81	1.7	1.8	2.2	2,9	5.6
8	83	2.4	2.6	3.0	4.0	7.2
10	86	3.1	3.3	3.9	4.8	9.2
12	90	3.7	4,1	4.8	6.0	11.3
15	92	4.7	5.2	6.1	7.5	14.0
18	96	5.5	5.9	7.3	9.1	17.4

The distribution of the dose absorbed in depth in a horizontal and a transverse plane on the electron beam is presented in Figure 14.

Plan A, parallel to the incident beam that passes through its axis, shows the isodose levels of 90, 85, 80, 70, 60, 50, 40, 30, 20, 10, the position of the dose D_m and the path $R_{50}/2$.

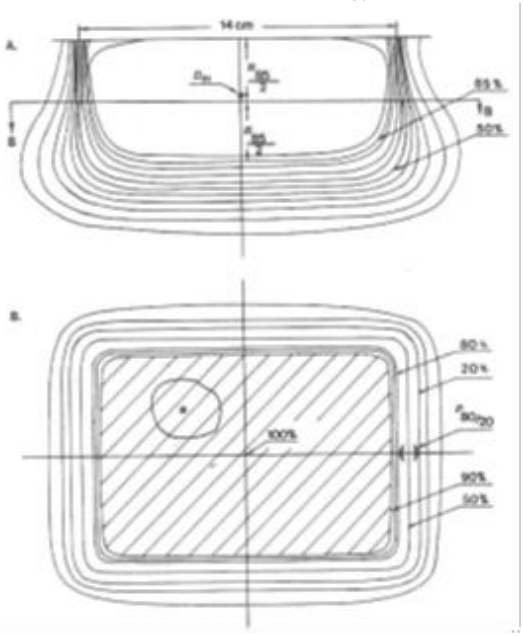

Figure 14: Absorbed dose distributions in two planes: parallel and perpendicular to the beam. ICRU 35, [27].

Plan B, perpendicular to the axis of the electron beam at a depth

of $R_{85}/2$, shows, in addition to the homogenization of the dose that is going to fall on the tumor, also the physical penumbra. This is defined as the average distance between two specified dose levels, for example the 80% and 20% levels, thus denoted $P_{80/20}$.

To have an overview of the dose distributions absorbed in depth at various energies, Figure 15 shows the dose distributions in depth on the beam axis, for energies of 4, 6, 9, 12, 15, 20 MeV.

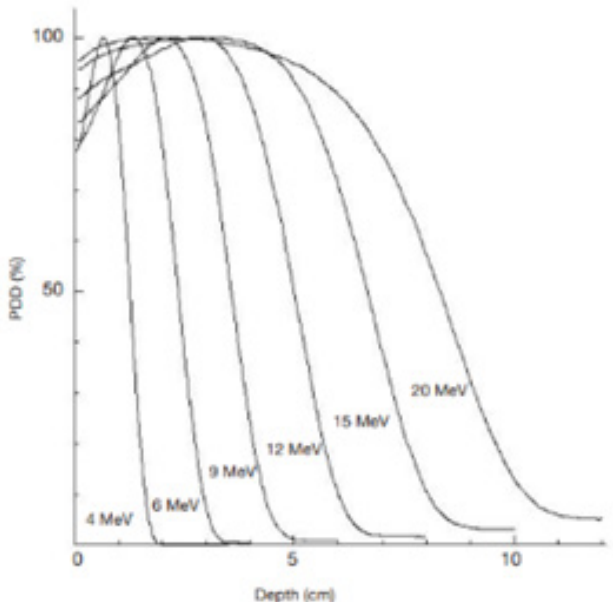

Figure 15: An example of central axis PDD curves for a family of electron beams from a high-energy linac, [22].

The quality factor of the electron beam represents half the value of the depth in the water **R_{50} (in g/cm²)**. This is the depth in water at which the absorbed dose is 50% of its value at the maximum absorbed dose at (SSD) of 100 cm and field size at the surface of the phantom of at least 10 cm x 10 cm for $R_{50} \leq 7$ g·cm², and for $R_{50} \geq 7$ g·cm^{-2}, at least 20 cm x 20 cm. Regarding the phantom material, for water $R_{50} \geq 4$ g·cm^{-2}, for water or plastic $R_{50} < 4$ g·cm^{-2}, and for water or plastic $R_{50} \leq 4$ g·cm^{-2}, [22].

The distributions are normalized to 100% at z max. Contamination with bremsstrahlung depends on the energy of the electron beam and the scattering folie. This is less than 1% for 4 MeV and less than 4% for 20 MeV. The distributions of the dose absorbed in depth corresponding to irradiation with electron beams, which at 20 MeV reach a depth of 10 cm, we could interpret them as representing the "BG peak" from hadrons upon entering the body in the first half (< 10 cm).

The difference lies in the fact that the dose at the entrance field, during electron irradiation, is between 81% and 96%, according to the data presented in Table 5, compared to the case of hadrons, which for the BG peak located in the second half of depth in the body, the dose from the entrance goes on a plateau of 20% until the peak.

Carbon/Proton beam therapeutical systems

Clasical cyclotron (B = const, f = const, ρ increase with energy).

E. O. Lawrence patents the method and the associated apparatus, called cyclotron, in 1931. The author received the Nobel Prize (1939) for "Invention of the cyclotron and results obtained with it, especially with regard to artificial radioactive elements".

Cyclotron is an accelerator that accelerates charged particles (protons, deuterons, α - particles and other ions) along a spiral trajectory in a vacuum chamber with the help of a radiofrequency (RF) electric field. This accelerator uses a constant magnetic field to guide charged particles to pass through the accelerating electric field at regular time intervals.

The energy gain or particle acceleration is based on the principle of resonance between the frequency of the RF voltage, $\omega_{RF,}$ applied on the duants to generate the acceleration electric field, and the frequency of rotation of the accelerated particle, ωrev
≡ qB/m0γ, that means ωRF = ωrev or

$$f_{RF} \equiv f_{rev} \equiv \frac{1}{T} = \frac{qB}{2\pi\, m_0\, \gamma} \ . \qquad (28)$$

Relation (28) shows that resonance occurs because the three quantities, frequency, magnetic field and mass of the ion are constant. The radius of the trajectory (ρ) in the spiral, increases with the energy of the particle according to the relation,

$$\rho = \frac{\gamma m_0\, v}{eB} = \gamma\, \beta\, \frac{m_0 c}{eB} \ . \qquad (29)$$

The resonance condition is preserved when the Lorentz factor is equal to unity, γ = 1. This means that classical cyclotrons can accelerate protons to kinetic energies below (20 - 30) MeV. Cyclotrons are characterized by the energy constant value, K, defined (nonrelativistically), by the maximum kinetic energy per nucleon,

$$\frac{T_m}{A} = \frac{p^2}{2m_u} = \left(\frac{Q}{A}\right)^2 \cdot K \ , \qquad (30)$$

where factorul K, related to the magnetic rigidity, it is

$$K\ (MeV) = 48.244\ \left(\frac{MeV}{T^2 m^2}\right) \cdot (B_{ave.} \cdot \rho_{ext})^2 \ .. \qquad (31)$$

Here we have: the impulse, p = Q e B ρ, corresponding to the extraction radius, $\rho_{ext,}$ q = Q·e is the ionic charge, A the atomic number, m = A m_u , $m_u = m_0/A = 931.5$ MeV/c² is the atomic mass unit, m_0 = is the rest mass of the ion, for the electron, the magnetic rigidity, mc/q = -1,705 Tm and for ion,

$$mc/q = 3{,}11\ (A/Q)\ Tm. \qquad (32)$$

Robert Wilson from Harvard University, starting from the depth absorbed dose distribution, in a water phantom, for a single proton and a proton beam, Figure 16**,** made the first proposal, according to which the accelerated protons should be taken under consideration for radiotherapy, 1946 [28].

His idea was realized in 1954, when 30 patients were treated with protons by Tobias and his colleagues, in the Lawrence Berkeley Laboratory. The main clinical requirements for proton and carbon ion therapy are presented in Table 5, [29].

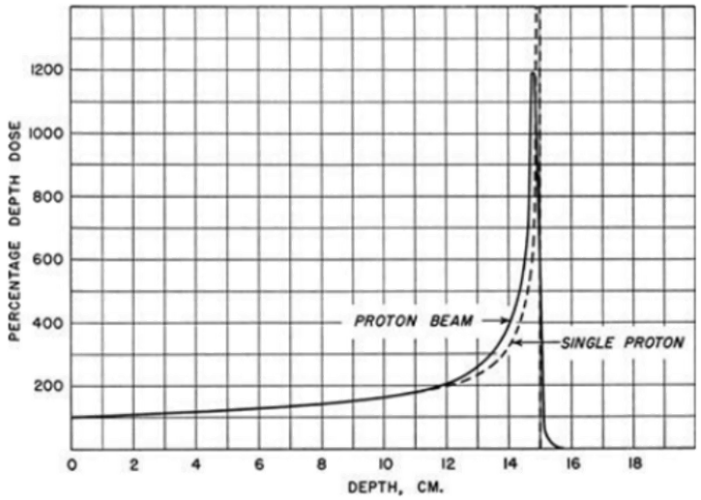

Figure 16: The original picture from R.R. Wilson [28].

Table 5: Protons and carbon ions 1662 [29].

Parameter	Value	Units
Extraction energy (proton)	60, 240	MeV
Extraction energy (carbon)	110, 450	MeV/u
Energy step (protons)	5, 1	MeV
Energy step (carbon)	15, 6	MeV/u
Energy resolution ΔE/E	3.5, 1.8	%
Voxel size	4×4×4, 10×10×10	mm
Smallest field of view	100×100, 250×250	mm
Clinical dose rate (proton)	2, >10	Gy/min
Clinical dose rate (carbon)	2, >10	Gy/min
Cycle rate	0.5, 2	kHz
Bunch charge (protons)	1.6, 16	p C
Bunch charge (carbon)	300, 3000	f C
Bunch charge stability and bunch charge measurement accuracy	<10 %	
a,b = values for min / max = minimum/maximum		

Proton beam therapy accelerator systems

Synchrocyclotron for proton therapy B = const, f varies, ρ increase with energy)

The possibility of resonant acceleration up to unlimited theoretical energies, when the resonance condition is respected, led to the application of a modulation of the cyclotron frequency to track the rotation frequency.

The synchrocyclotron differs from the classic cyclotron by two changes. The first refers to the magnetic field gradually decreasing with radius, (dB/dρ) < 0, to achieve a vertical focus,

$$0 < n \equiv -\frac{\rho}{B}\frac{dB}{d\rho} < 1, \quad (33)$$

and second, the RF frequency gradually decreases with time to compensate for the decrease in magnetic field and increase in particle mass,

$$\omega_{rev} = \frac{qB}{\gamma m_0} = \omega_{RF}\,. \quad (34)$$

Through frequency modulation, both the effect of the increase in mass and that of the decrease in the field necessary for vertical focusing are compensated.

The first synchrocyclotron (UCRL Berkeley, 4.7 m, 4300 t, p: 350MeV) was built in 1946, about a year after the discovery of the principle of phase stability (or the synchrotron accelerator) by Veksler (1944) and Mc Millan (1945). The principle consists in the existence of closed orbits inside the separatrix, and the finite phase space admittance (acceptance) of an accelerator.

The limiting curve of particle trapping in the phase space is called a bucket. The particles inside the bouquet perform oscillations around the center of the potential well, called synchrotron oscillations. They appear as closed curves in the phase space. Whereas the cyclotron can accelerate a stream of particles, the synchrocyclotron can only accelerate one “bunch” of particles.

One such example is 230 MeV superconducting synchrocyclotron (S2C2) for proton therapy presented in Figure 17, [30].

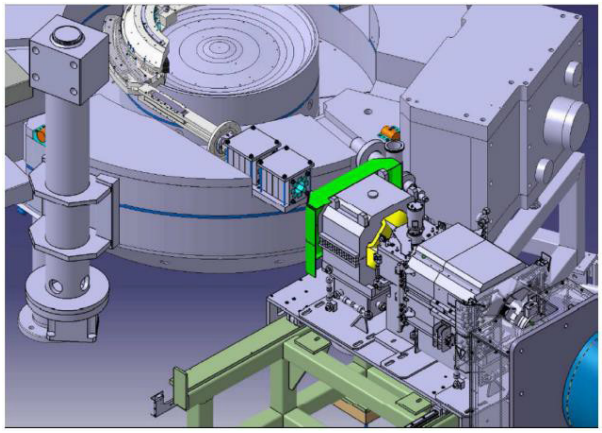

Figure 17: A view of the medical synchrocyclotron S2C2 [30].

Its main parameters are presented in Table 6, [31,32].

Table 6: Main parameters of the S2C2 synchrocyclotron.

Proton final energy	230 MeV
Beam intensity	20 nA / 400 nA
RF frequency	93 -63 MHz
Peak dee voltage	11 kV
Magnetic field: central / extraction	5.7 T / 5.0 T
Final radius	500 mm
Cyclotron diameter	2500 mm
Cyclotron height	1600 mm
Cyclotron weight	50 t

Isochronous Cyclotron (B varies, f = const, ρ increase with energy)

The main disadvantage of the synchrocyclotron consists in the reduced average beam intensity extracted at the end of the acceleration of 10^{-3} 10^{-4} times lower than that extracted from the injection source.

The isochronous cyclotron removes this disadvantage by maintaining the resonance condition at a fixed acceleration frequency by giving up the weak magnetic focusing and using alternating azimuthal focusing, for vertical stability, making the directing field increase with the radius, $(dB/d\rho) > 0$, i.e., $B = B_0\gamma$, so that the rotation frequency of the particle is constant,

$$\rho = \frac{\gamma m_0 v}{eB(\gamma)}. \quad (35)$$

As an example, we mention the IBA C 235 cyclotron, for Proton Beam Therapy. Gantry Treatment Rooms are presented in Figure 18, [33]. This contains spiral sectors.

Figure 18: Gantry Treatment Room of the IBA Proton Therapy System.

The equivalent of clinical parameters in proton accelerator parameters is presented in **Table 7.**

Table 7. Main parameters of Cyclotron C 235.

Proton final energy	230 MeV
Beam intensity	300 nA
Magnetic field: central / extraction	1.74/2.2T
RF frequency	106 MHz
Peak dee voltage	150 kV
Diameter	4.34 m
Cyclotron height	1600 mm
Weight	210 t

Medical Proton Synchrotron (B varies, f varies, ρ = const)

In the synchrotron, the particles are accelerated along a circular trajectory, with approximately constant radius, Bρ = <B>R = p/q, where ρ is the radius of curvature of the dipole and R is the radius of the circular orbit of the synchrotron. The operating principle is based on the resonance between the rotation frequency of the synchronous particle, ω_{rev}, and the acceleration frequency, ω_{RF}/h, h = harmonic number = number of possible "bunches", ωs = ωRF/h = (q/m) <B> = (q/m).(ρ/R).B.

The operation of the cyclotron in "slow cycle" regime is ensured by the linear increase of the magnetic field from the value B (injection) to B (fixed energy), and for the operation in "fast cycling" regime, the magnetic field is modulated harmonically (≥ 3 Hz).

Longitudinal stability consists in the existence of a particle of synchronous energy E_s, momentum p_s, rotation frequency f_{rev}, phase RF Φ_s, and azimuthal angle θ_s, from a beam and the rest of the particles in the beam perform stable synchrotron oscillations around the synchronous phase, with deviations, corresponding to the synchronous particle, not greater than ΔE, Δp, ΔΦ, Δf and Δθ.

The particle trajectories obtained in the phase space, energie ($\equiv \Delta E/f_{rev}$) vs Φ position are presented in Figure 19 **[34]**.

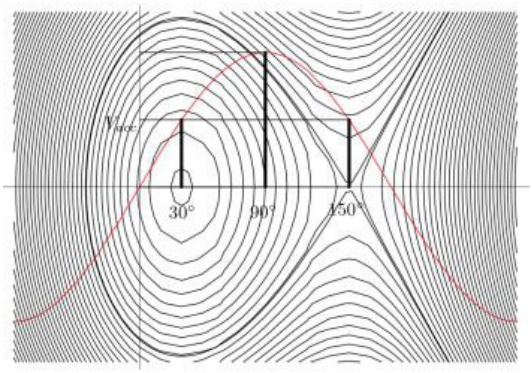

Figure 19: The particle trajectories obtained in the phase space.

This case corresponds to the particle acceleration process (sin Φs > 0) because the stable phase is $\Phi s = 30^0$, a stable fixed point, and π—$30^0 = 150^0$, represent an unstable fixed point, corresponding the separatrix. The limit curve of the particles captured in the phase space is called the RF bucket. Separatrix is curve in phase space separating stable from unstable region.

The area of the RF bucket is given by the formula,

$$A\ (\text{eV. s}) = \frac{16}{2\pi}\frac{\beta}{f_{RF}}\alpha\ (\Phi_s)\sqrt{\frac{e\,\hat{V}_{RF}E_s}{2\pi\ h/\eta/}}\ , \quad (36)$$

where is the frequency slip factor, and α (Φs) is a function that characterizes the accelerator bucket, the rest of the quantities being defined above.

In the small-amplitude approximation, the longitudinal emittance, or phase-space area of a bunch of particles in terms of the bunch length, is given by **[35]**,

$$A_s\ (\text{eV.s}) = \pi\ \breve{W}\ \Delta\Phi = \pi\ (\Delta\Phi)\frac{e\bar{V}\cos\Phi_s R_s p_s}{2\pi h(-\eta)\Omega_s}\ . \quad (37)$$

The longitudinal emittance of the beam, $\in = A_s/\pi$, has dimensions of energy x time, and it is constant during the acceleration period.

Longitudinal stability ensures the length of the bunch, while transverse stability determines its height and width.
In this paragraph we will give two examples of hadron sources for

Medical Synchrotron. From the category of proton synchrotrons, which have a radius between 6-9 m, we chose a synchrotron that, from the energy point of view, falls within the recommendations of the IAEA, TRS 398, 50 – 250 MeV.

Example 1: The synchrotron for proton therapy with proton energy between 70-250 MeV HITACHI. An overview is given in Figure 20.

Figure 20: A view of Proton Synchrotron of 70 –250 MeV, [36].

Table 8: The main parameters of proton synchrotron.

Proton energy for passive	70 - 250 MeV	
Proton energy for scanning	70 - 220 MeV	
RF frequency for extraction protons	0.7 – 1.1 MHz	
Repetition frequency	2 – 7 s	
Extracted beam	0.5 – 5 s	
Efficiency transport ofthe proton beam	90 %	
Dose of 2 Gy in the tumor	2,7 x protons	1011
Radius	~7 m	
Weight	~15 – 20 t	

Example 2, also represents a source of carbon ion beams that falls within the IAEA recommendations, with kinetic energy between 1200 MeV (or 100 MeV per nucleon) and 5400 MeV (or 450 MeV per nucleon). It is about synchrotrons of heavy ions.

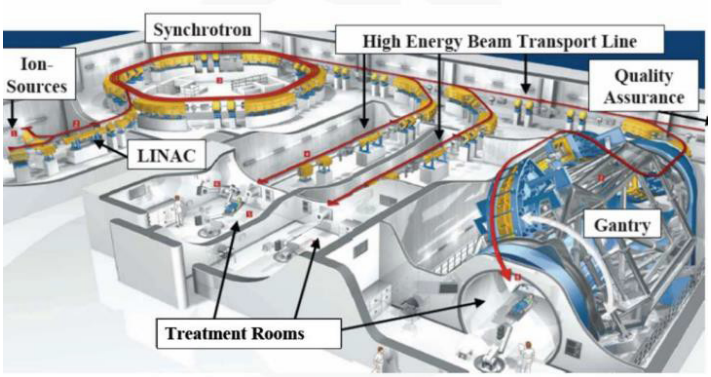

Figure 21: Synchrotron of Carbon Ions. HIT: Heidelberg Ion Therapy Facility [37].

These accelerators have a radius of 19 - 25 m. This type of accelerators has the advantage of lower weights (< 200 t) due to the fact that the radius is constant during the acceleration process, the magnetic field for maintaining the equilibrium orbit exists only in its vicinity to cover the betatron oscillations of the beam of charged particles. Synchrotron Technology for Carbon Ion Beam is presented in Figure 21.

The picture shows the complexity of the treatment system composed of the following technologies: ion sources for linac, which together with the linac represents the injection subsystem for the synchrotron, the synchrotron that supplies proton and ion beams, high energy transport line, three treatment rooms, of which two are for protons and one for ions, in which the gantry corresponding to the beams is located.

The irradiation main parameters for protons and carbon ion beams in the treatment of cancer are presented in Table 9 [38].

Table 9: Some parameters for protons and carbon ions.

Parameter	Steps	Protons	Carbon
Energy	255	48 - 221 MeV/u	88 – 430 MeV/u
Focus	4 (6)	8 - 20 mm	4 - 12 mm
Intensity	10 (15)	8.10^{7}- 2.10^{10} i/s	2.10^{6}-5.10^{8} i/s
Places	5	5	5

Table 9 shows that Heidelberg Ion Therapy (HIT) uses 4 ion species for the treatment of malignant tumors: protons, helium-, carbon- and oxygen-ions; 255 energy steps; and 10 [up to 15 steps) of intensities expressed in ions per second. In total, 91,800 combinations are made (not taking into account beam source, beam target and gantry angle).

These parameters are provided by the HIT Synchrotron medical accelerator which has the following main parameters: circumference: 64.986 m, and magnetic rigidity B:1.1 – 6.5 Tm.

Clinical Proton Beams

IAEA TRS 398 recommends, for proton radiotherapy, proton beam systems with kinetic energy between 50 MeV and 250 MeV.

The energy of the particle determines its penetration depth in the patient. Depending on the energy value, the distance varies between 0.5 cm and 32.5 cm. At the minimum energy (50 MeV) they correspond: $\gamma = 1.05$, $\beta = 0.314$, pc = 310 MeV si $B\cdot\rho = 1.02$ Tm, and at maximum energy (250 MeV), correspond to: $\gamma = 1.27$, $\beta = 0.614$, pc = 729 MeV and $B\cdot\rho = 2.43$ Tm.

The intensity of the beam current in nA (or the flow of particles) determines the absorbed dose, administered in the tumor. Considering that the energy, 1 MeV = 1,602 x 10^{-13} J, the charge of the proton, $q \equiv e\cdot Q = 1.602 \times 10^{-19}$ C, and 1 C = 3 x 10^{9} e.s.u., the result is the value of the current in the number of protons per second,

$$1\ \text{nA} = 10^{-9}\ \frac{C}{s} \cdot \frac{p}{1.602\ x\ 10^{-19} C} = 6.24 \times 10^{9}\ \frac{p}{s}\ . \qquad (38)$$

The power of the beam when the intensity of the current was known is given by the relationship,

$$P\ (W) = E\ (MeV) \times I\ (nA)\ . \qquad (39)$$

The number of ionized atoms N (≡ i.a.), or the number of ion pairs (i.p. = i.a.), in a mass of normal tissue, m = 1 kg = 1 L = 1000 cm^3, for a dose of 1 Gy, is calculated with the relation

$$\frac{N}{m} = \frac{D(Gy)}{W(J/i.p.)} = \frac{6.24\ x\ 10^{18}\ eV/kg}{34\frac{eV}{i.p.}} = 1.83 \times 10^{17}\ i.a./kg\ . \qquad (40)$$

For 1 Gy of absorbed radiation dose in tissue, using the equation (40) results: 1,83 x 10^{14} i.a./g and 10^5 ionized atoms within the volume of every cell of diameter 10 μm. For 1 R, we have 1.61 x 10^{12} i.a./g of air, and 2,09 x 10^9 i.a./cm^3 of air.

Depth-dose distribution

A typical, natural, depth dose distribution for a therapeutic proton beam is shown in Figure 22 [13].

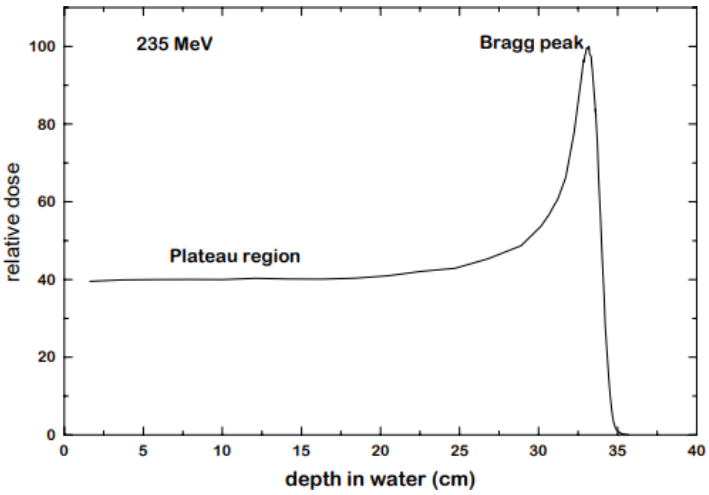

Figure 22: Percentage depth-dose distribution for a 235 MeV proton beam.

This has a plateau region, followed by the location where the most energy is rapidly released, up to a maximum, called the "Bragg peak".

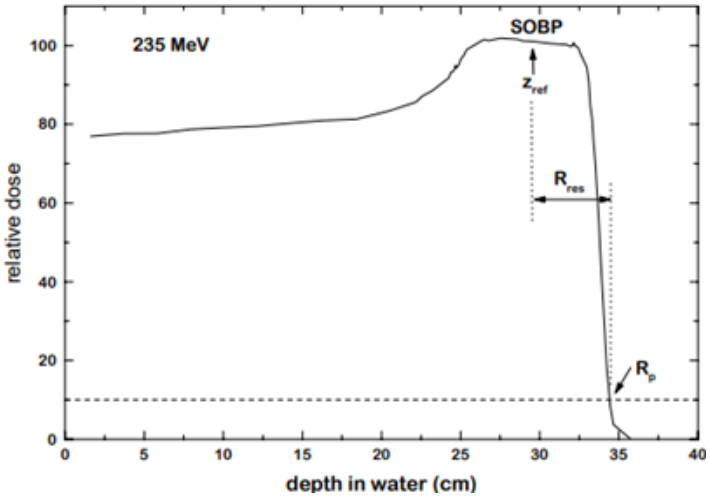

Figure 23: Percentage depth-dose distribution for a modulated proton beam. SOPB (Spread Out Bragg Peak).

Proton beam quality specification R_{res}

The typical depth dose distribution for a clinical proton beam with a SOBP is given in Figure 23.

In this, the following are indicated: - the practical range R_p, defined as the depth at which the dose beyond the Bragg Peak or SOBP drops to 10% of its maximum value, - the reference depth z_{ref} (middle of the SOBP), - the residual range at z_{ref}, used to specify, - the quality index of the beam, R_{res}, defined by relation (41),

$$R_{res} = R_p - Z_{ref}\ . \qquad (41)$$

Here, the depth chosen for measuring the dose, z_{ref}, and the practical path, Rp, are both expressed in g / cm^2.

The processing of the proton beam with a kinetic energy of 250 MeV, energy fine degrader to obtain energies between 50 - 250 MeV and the assembly for measuring the quality index R_{res} are presented in Figure 24.

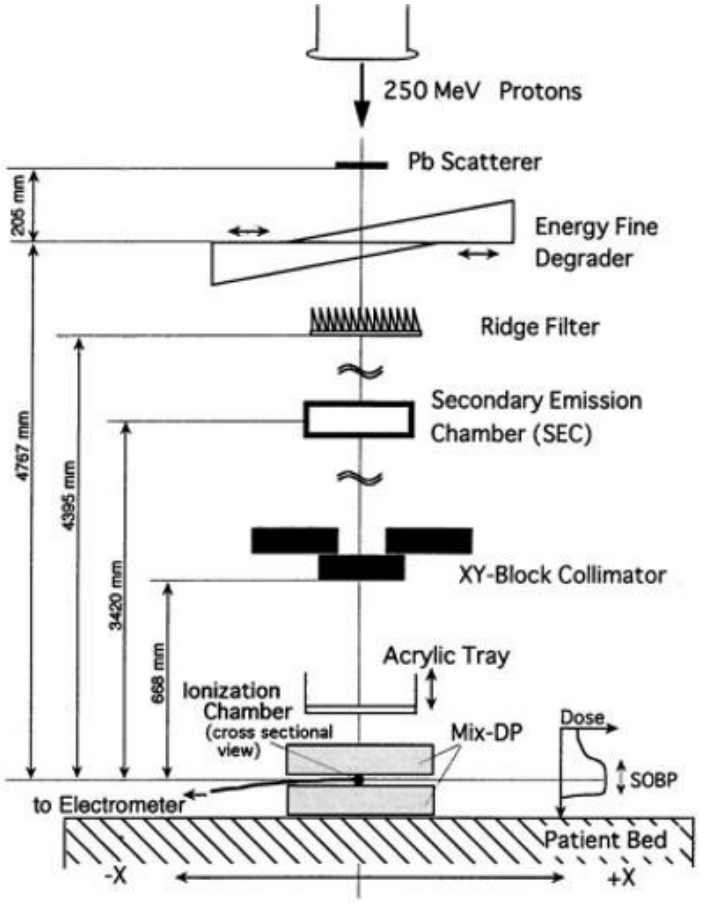

Figure 24: Experimental arrangement for proton irradiations at the vertical irradiation line of PMRC, [39].

Heavy ion beams therapeutical Systems

The physics of carbon-ion beams is similar to that of proton beams (a plateau at the entrance point of the beam, followed by a sharp rise in dose at the end of the path, at the Bragg peak), but the mass of carbon ions is much greater.

Absorbed Dose, D = 1 Gy = 1 J/kg = 6.24 x 10^{12} MeV/ (kg = L = 1000 cm^3). Therefore, for 1Gy in 1 litre of tumor, we need 5,2 GeV carbon ions (c.i,), each of 1200 MeV, or 5.2 x 10^9 c.i, and 190 MeV carbon ions, each of 5400 MeV, or 1,1 x 10^9 c.i. for the treatment of malignant tumors.

In terms of beam currents, 0.1- 0.2 nA for carbon ions corresponds to a typical dose rate of 2 Gy in 1 L, in one minute.

The code of practice applies to heavy ion beams with atomic numbers between 2(He) and 18(Ar) having ranges from 2 g cm^{-2} to 30 g cm^{-2} in water. For a carbon beam, this corresponds to a range of kinetic energies from 1200 MeV or 100 MeV/u (energy per nucleon), crossing 2.58 cm, to 5400 MeV or 450 MeV/u (energy per nucleon), crossing 33.65 cm in water, [22].

The distribution of the absorbed dose in depth in water for proton kinetic energy of 160 MeV and for carbon ion energy of 260 MeV/u, where u is the atomic mass unit, 1 u = 931.5 MeV/c^2 = 1.660 x 10^{-27} kg is presented in Figure 25, [40].

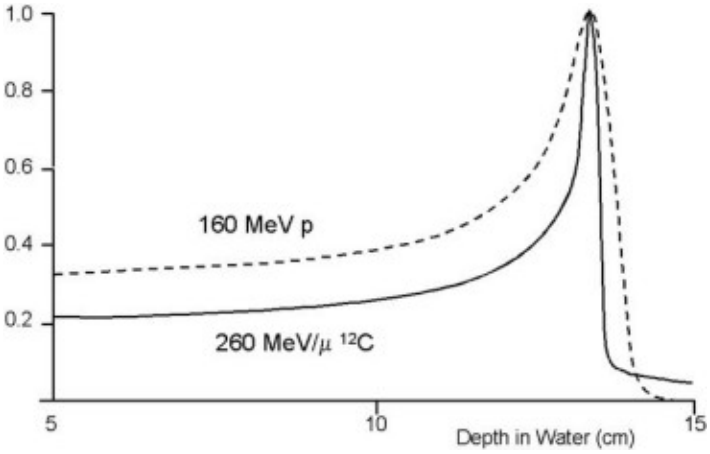

Figure 25: Depth dose distribution for a monoenergetic 160 MeV proton and 260 MeV/u carbon ion in water [40].

Comparing the two distributions, the following results: 1. characteristic is the Bragg peak, which is more pronounced for carbon ions; 2. the distal dose gradient is steeper for ions; 3. the ratio between the Bragg peak dose and the dose in the entrance region (plateau) is higher for heavy ions than for protons; 4. Protons have a finite path, compared to ions, where there is an extension of the dose behind the Bragg peak (the so-called fragmentation tail), no higher than 10% of the target dose.

Clinical applications require a relatively uniform dose to be delivered to the tumor volume and, for this purpose, the proton beam must be homogenized both horizontally and vertically. This is achieved at a treatment depth by superimposing Bragg peaks of different intensities and energies. The technique is called "beam modulation" and creates a region of high dose uniformity called a "spread Bragg peak" (SOBP), Figure 26 [41].

The effects of equal doses of different types of radiation produce unequal biological effects. The comparison of the effects of different types of radiation is expressed as relative biological effectiveness (RBE).

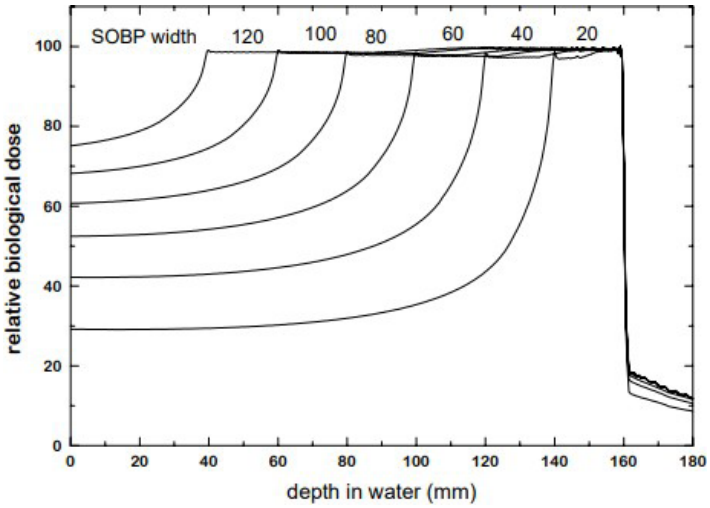

Figure 26: Biological dose distributions of therapeutic carbon beams of energy 290 MeV/u. SOBPs of 20 to 120 mm width are designed to yield uniform biological effect in the peaks [41].

This is defined as the ratio of dose of a reference radiation quality (usually 250 keV – X rays, of low LET) and dose of a test radiation (of higher LET) that produce equal effect.

The distributions for proton and neon, normalized to the peak of the carbon ion, are shown in Figure 27 [42].

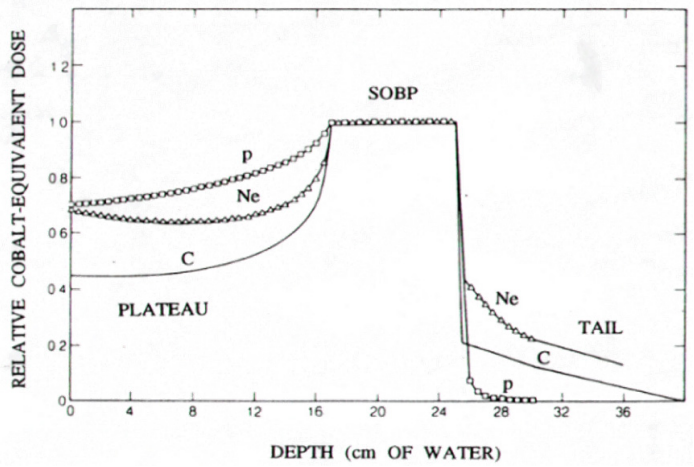

Figure 27: Central axis depth dose profiles from several particle beams: p, C, Ne, [42].

It is clearly seen in this figure that only the proton distribution is reduced to zero, while the neon and carbon ion distributions have large tails after the end of the Bragg Peak.

At the end from the homogenization system of the proton beam, which coincides with the entry surface in the phantom of water, the dose distribution, homogenized horizontally and vertically, has the form of Figure 28 [43].

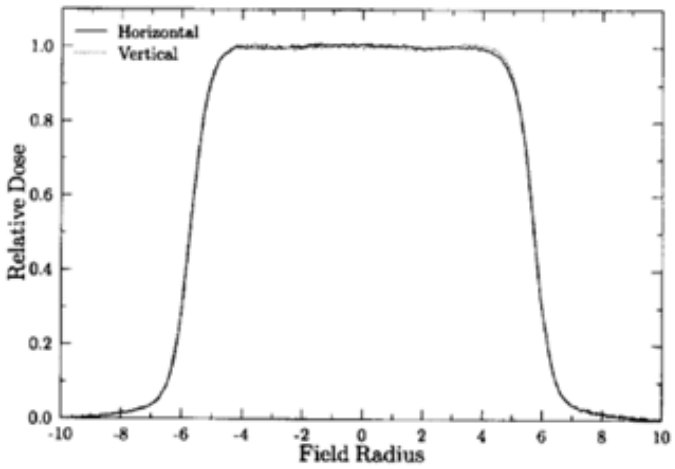

Figure 28: An example of dose profiles in orthogonal transverse directions near the center of 10-cm range modulation for a 250-MeV treatment field [43].

Scanning irradiation systems for therapy

The radiation beam provided by a medical accelerator, at the end of the acceleration period (or at the extraction window) is cylindrical in shape with a diameter of a few mm and a narrow energy spectrum. There are two methods of forming the beam, in addition to spreading and homogenizing the beam at the level of the irradiation fields, must ensure the variation of the supplied energy depending on the depth at which the tumor is located and the distribution of the absorbed dose only in the volume of the target tumor and very little or not at all in the adjacent areas. The principle of the two methods is presented in Figure 29 [44].

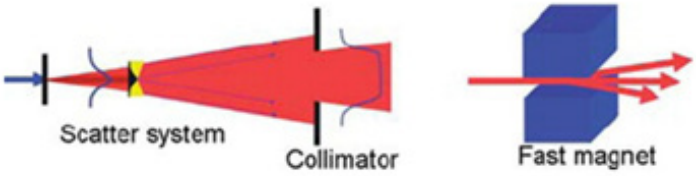

Figure 29: The two methods to spread the beam in the transverse plane: scattering (left) and pencil beam scanning (right) [44].

The first method, the passive beam shaping method, is based on properly processed metal (static) components. Second, the active beam shaping method (or active pencil beam scanning method) is based on the magnetic rigidity of the particle beam for the variation of the beam energy in the accelerator and the transverse extension of the beam. The scanning mode can be discrete (pixel scanning) or continuous scanning (raster scanning), which currently lead to almost identical results.

Passive-dose delivery system

The principle of the passive – dose delivery system used for proton and ion beams is presented in Figure 30.

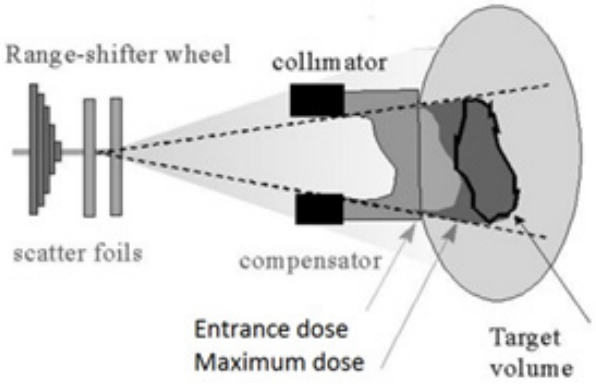

Figure 30: Principle of the passive dose-delivery system used for charged particle therapy [45].

As with photon intensity modulated radiation therapy (IMRT), intensity modulated proton therapy (IMPT) uses multiple ports. Each port is designed with an inhomogeneous proton fluence distribution so that when all fields are combined, a homogeneous dose is delivered to the target volume. The passive supply mainly consists of placing in front of the patient absorbents that change the characteristics of the beam.

The fixed part of the passive method includes the variable range shifter has to shift the depth dose to the desired and the spreading system with two scatter foils to enlarge the beam. The variable part of the method, specific to each angle of incidence of the beam on the tumor, includes the multileaf collimator and a compensator that adapts the distribution of the absorbed dose to the size and distal shape of the target volume.

This method has the advantage that it is practically independent of the movement of the target organs during the irradiation, being the most used nowadays. Spreading the Bragg peak to a certain depth is achieved with the help of a rotating wheel, which is placed in the beam with the axis of rotation parallel to the beam direction.

Active-dose delivery system

The principle of the active raster scanning system used at GSI for carbon ions este schitat in Figure 31. A small pencil beam is scanned in vertical and horizontal direction using 2 pairs of scanning magnets.

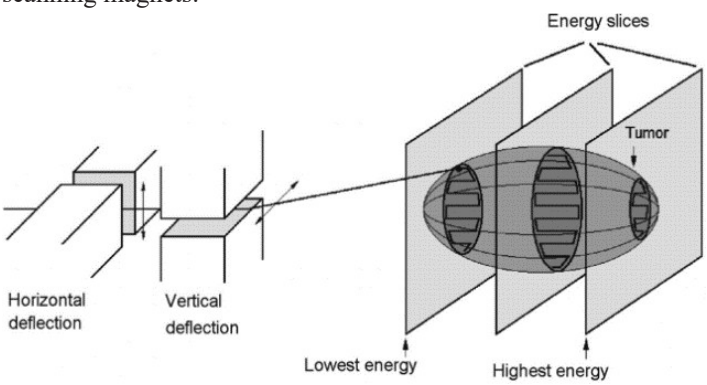

Figure 31: Active raster principle used at GSI for carbon ions, [46].

Active scanning was first used in Japan in 1980 and then optimized and regularly used for treatments at PSI, GSI, HIT and CNAO.

A small pencil beam is scanned in vertical and horizontal direction using two pairs of scanning magnets. For scanning, the tumor is divided into slices in the longitudinal direction. It is assumed that each slice consists of small volumes called voxels (or patches). The beam energy is determined by the depth of each slice. Each voxel in the slice is irradiated by changing the currents of the scanning magnets. The depth at which the second slice is located is selected, the beam energy is fixed, and all voxels are irradiated, after which the process is repeated. Pencil beam scanning offers the best flexibility for dose distribution modeling. When continuous scanning is used, the beam is swept along a contour or line while varying the intensity of the beam. The active scan method allows for News Conventional Technologies of Proton Therapy.

An example of calculating the dose distribution for the scattering and scanning methods is shown in Figure 32 [45].

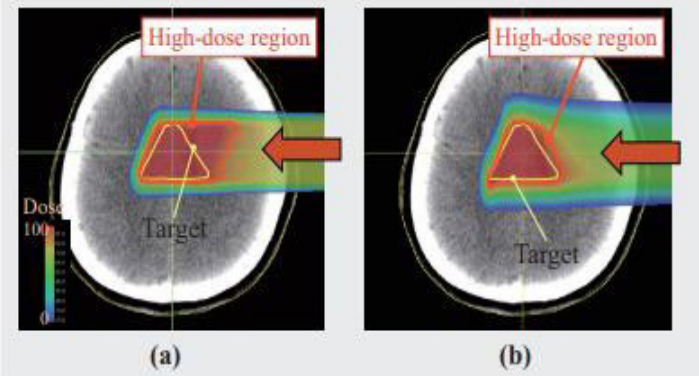

Figure 32: Scanning method. Comparison of dose distribution in scattering and pencil beam scanning method, [47].

This shows how the high-dose region (region shown in red) formed by the scanning method matches the target shape (indicated by the yellow line) better than the scattering method.

News Conventional Technologies of Proton Therapy

Synchrocyclotron accelerator technology

To reduce the area that must be covered by the magnetic field, the 250 MeV Still River superconducting proton synchrocyclotron, using a magnetic field of 9 T, reaches the weight of the proton accelerator of about 20 tons, for the extraction radius of 25 cm, Figure 33 [47].

Pricipal parameters are presented in **Table 10.**

Table 10: Main synchrocyclotron parameters.

Final energy	250 MeV
Beam intensity	40 nA (100 nA design)
Magnetic field: central/extraction	8.9 T/8.2 T
Extraction type	Self extraction
Cyclotron diameter	1800 mm
Cyclotron height	1600 mm
Cyclotron weight	25 t

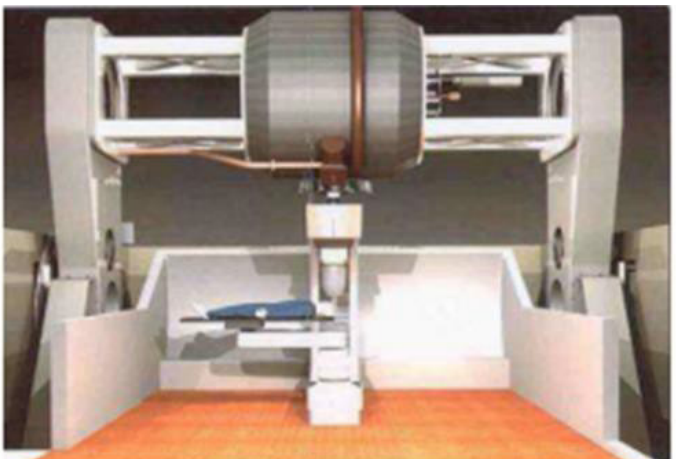

Figure 33: Superconducting Synchrocyclotron with 9T field built by "Still River".Weight is 20 tons [48].

Isochronous Cyclotron (radioresistant tumors)

The IBA C400 accelerator differs from the standard isochronous cyclotron with B = 1.8 T in that it uses superconducting magnet technology that ensures a magnetic field B = 4 - 5 T to reduce volume and weight Figure 34, [48].

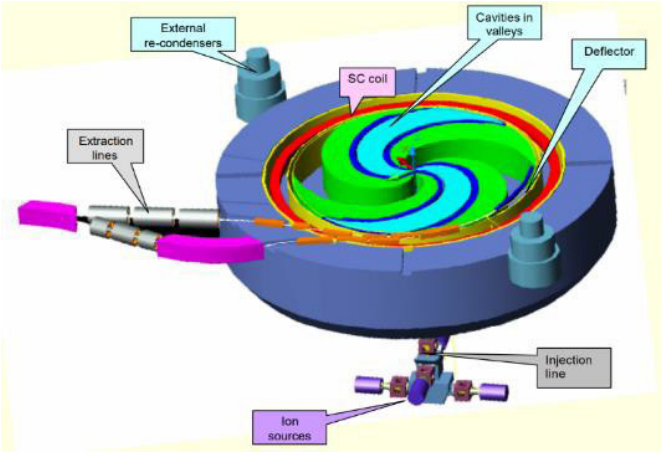

Figure 34: View of the cyclotrom C 400, [49].

Table 11: Main parameters of the C 400 cyclotron.

Parameter	Value
Cyclotron type	Compact, Isochronous
Accelerated particle	H^+, 24H2+ , 12C6+
Final ions/protons energy:	400 MeV/u/265 MeV/u
Carbon beam intensity	8enA
Injection type	ECR ECR, multi-cups
Central magnetic field	2.5 T
Sector shim ttype, spiral angle	Archimedean spiral, 73^0
RF systm	Two spiral cavities
Operation RF harmonic	4
RF frequency	75 MHz
Peak dee voltage: center /extraction	80 kV /160 kV
Final radius	1850 mm
Extraction ions/protons type:	Deflector/ Striping foil
Cyclotron diameter	6600 mm
Cyclotron height	3400 mm
Cyclotron weight	700 t

FFAG accelerators (B constant in time and varies with radius, f varies, ρ increases with energy)

The principle of FFAG acceleration is based on the use of cavities to give energy to particles that cross each other several times during their circular motion, in an area with a constant magnetic field that guides the charged particles along a closed orbit. At each rotation, the particle gains energy, through the associated momentum. After a particular number of rotations, it reaches the programmed kinetic energy.

From the point of view of the magnetic field, circular accelerators are of four types: fixed-field constant-gradient accelerators, including conventional cyclotrons, synchrocyclotrons, and microtrons; pulsed-field constantgradient accelerators, which includes weak-focusing synchrotrons and betatrons; pulsed-field alternating-gradient accelerators, which are the well-known AG synchrotrons and fixed-field alternating-gradient accelerators, otherwise known as FFAGs.

The FFAG accelerator (B constant in time and it increases with radius, f varies, ρ increase with energy) is a ring accelerator with a constant magnetic field in time (FF) and an increase with variable frequency radius like the synchrocyclotron and alternating gradient (AG) like the synchrotron. The magnetic field profile is given by the relation $B_z = B_{z,0} (r / r_0) k$ where r and z are radial and vertical coordinates, respectively, the suffix 0 denotes the reference value and k is called the field index.

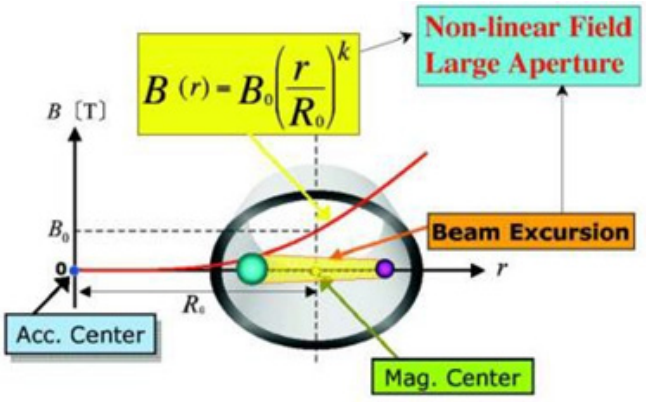

Figure 35: Magnetic field variation with respect to the radial coordinate for an FFAG, [29].

Two types of magnets are distinguished: linear when k=1 and non-linear when $k \neq 1$. If in the isochronous cyclotron the field had to increase with the increase of the Lorentz factor to maintain resonance, in the case of FFAG, there are no limits. There are two types of accelerators: Scaling FFAG that respects the scaling rule and non-scaling FFAG that doesn't respect it. Also, there are two types: FFAG with radial sectors and FFAG with spiral sectors. For medical therapy, NS FFAG Spiral was chosen, which is more compact and the magnetic field in a spiral FFAG generally has the form, $B(r, \theta) = B_0 (r / r_0)^k f(\vartheta)$, where we call ϑ a generalized angle [50].

FFAG accelerators have the potential to offer the benefits of both high current cyclotrons and synchrotrons, providing: - variable energy extraction; - high frequency of repetition, which leads to the rapid delivery of the absorbed dose. They have simple and stable operation thanks to fixed magnetic fields.

The main clinical parameters of FFAG NS Pamela are presented in Table 12 [51].

Table 12. Main clinical requirements of PAMELA

Extration energy: p	60 – 240 MeV
Extration energy: C	110 – 450 MeV/u
Energy step	1 – 5 MeV
Energy resolution	1.8- 3.5 MeV
Voxel size	4 x 4 x 4 -10 x 10 x 10 mm
Dose field size	100 x 100 – 250 x 250 mm
Dose rate: p	2 – 10 Gy/min
Dose rate: C	2 – 10 Gy/min
Dose rate: p	1.6 -16 pC
Dose rate: C	300-3000 fC
Repetition rate	0.5 – 1 kHz

News acceleration technologies driven laser

Laser driven plasma wake field accelerators – LWFA.

The operating principle of (LWFA) is based on the ponderomotive force associated with a laser pulse of duration τ that propagates through the underdense electron plasma ($n_e/n_c << 1$, $n_c(1\mu) = 10^{21} cm^{-3}$), with the refractive index n_p, and the wavelength λ_p.

Acceleration occurs when the duration of the intense pulse (drive pulse > $10^{18} W/cm^2$), is less than half the plasma wavelength, $c\tau < \lambda_p/2$.

Figure 36 shows a schematic representing (1) bubble formation when a high-intensity laser interacts with the plasma, (2) electron cloud generation around the bubble, and (3) electron self-injection behind the bubble. A short laser pulse with a duration of τ~(1/ωp) can form a plasma bubble, which is a nonlinear burst plasma structure comparable to an ion channel.

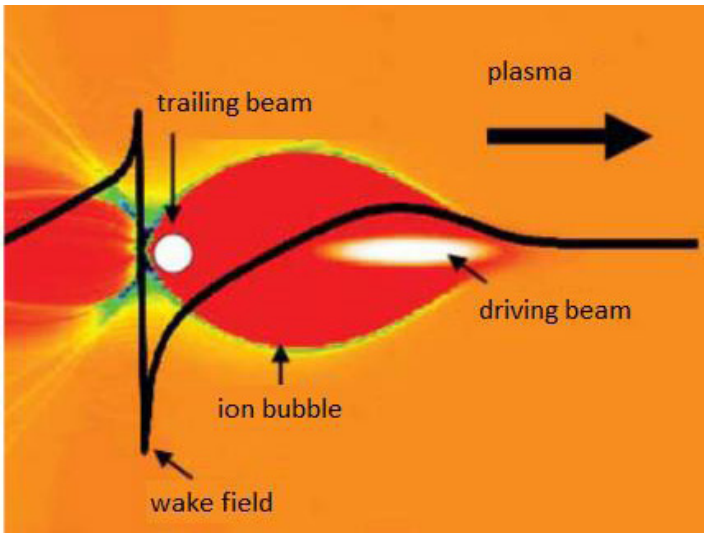

Figure 36: Schematic representation of the longitudinal wake field (black line) and ion distribution (red area) behind a driving laser or particle beam, [52].

The maximum energy T_{max} that can be obtained by electrons in a plasma wave is given by the product between the longitudinal electric field of acceleration associated with the plasma wave, E_p, and the acceleration length, L_{acc},

$$T_{max} = e\, E_p\, L_{acc}\ . \qquad (42)$$

There are three factors that limit acceleration distance and maximum power gain T_{max}: laser depletion, dephasing, and diffraction of the laser pulse. These limitations that refer to the "drive beam" do not raise problems for the realization of a "laser wake field acceleration", in the "bubble regime" of 4 - 25 MeV. Currently a LWFA can reach the energy of 1 GeV in ~ 3 cm, high peak current > 10 kA and ultra-short bunch < 50 fs, [53].

Example. The LWFA parameters for a intraoperative clinical application of a linac-laser accelerator (CEA Saclay), are presented in Table13 [54].

Table 13.

	IORT NOVAC	Laser - Linac
Company	Sardinia SpA	(CEA-Saclay)
Energy electron (MeV)	10	45
Available energies (MeV)	3, 5, 7, 9	5 - 45
Peak current	1.5 mA	>1.6 KA
Bunch duration	4 μs	<1ps
Bunch charge (nC)	6	1.6
Repetition rate (Hz)	5	10
Mean current	30 nA @ 10Hz	16nA@10 Hz
Released En in 1 min	18 J @ 9 MeV	21J@20 MeV

The parameters of the proposed accelerator, show the transition from μs technology (10^{-6} seconds) to ps technology (10^{12} seconds) [54].

Proton and ion acceleration

The basic principle of the "Target Normal Sheath Acceleration" (TNSA) mechanism, which leads to the acceleration of protons and ions, is presented in Figure 37 and described in [55].

A relativistic laser pulse with the laser strength parameter, $a_0 > 1$, incident on a thin target metal foil with a thickness of the order of microns, accelerates the electrons from the target surface in the direction normal to the target.

Fast electrons from the laser plasma penetrate a thin solid target and are emitted at the back. A strong quasi-static electric field is formed between the electron group and the ionized target, which normally acts on the metal surface has cylindrical symmetry and decreases in the transverse direction. Due to the ultrashort lifetime of the electron bunch and its high charge close to the axis, the quasi-static electric field can reach values of a few TV/m. Surface-abundant protons in the form of contamination layers will be accelerated along the field gradient in a well-defined manner. Experimental research conducted so far with Laser intensity > 10^{19} W/cm^2, pulse length: 10 -100 fs, and a few μm Titan target indicate the following achievements Maximum energy: protons ≈ 67 MeV, carbon ions ≈ 40 MeV/u.

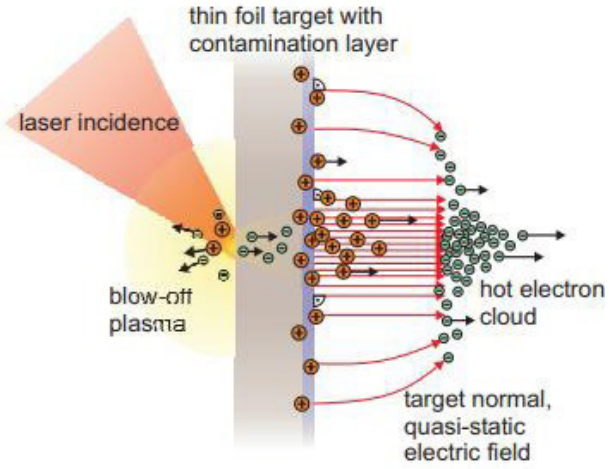

Figure 37: Target Normal Sheath Acceleration (TNSA), [55].

The Radiation Pressure Acceleration mechanism (RPA) for the acceleration of the ions in the plasma under the radiation pressure, it is based on equality between the energy density (7) and the radiation pressure. This is directly proportional to the intensity of the laser radiation (I), that is, $P_{rad} = 2I/c$. For thick targets at ne ≥ nc, the radiation pressure acts to push the electrons into the target, creating a critical surface in the plasma. Over time, the laser pressure will continue to press the critical surface into the plasma, causing the ions to accelerate due to charge separation at the laser front. For electron acceleration, the laser field intensity is 10^{18} W/cm^2, and in the case of ion acceleration, it is 10^{24} W/cm^2. The study carried out for acceleration in the so-called "laser piston" regime is presented in detail in works [56,57].

The functions dose vs depth, range vs energy, depth and tumor location vs particulate energy are presented in Figure 38 [58].

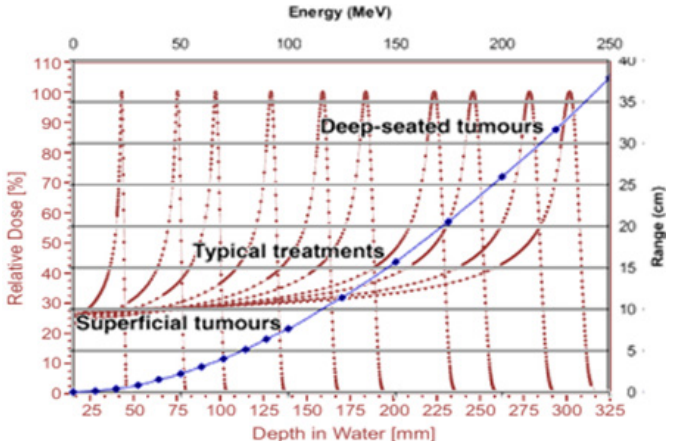

Figure 38: Dose vs depth in water and range vs energy deposition for proton beam treatment plane assessment.

An example of the conceptual gantry device for a general purpose ion accelerator, code, PARMILA, designed within the Photo Medical Research Center (PMRC) of JAEA, Kyoto University, Figure 39, is described in the paper [59].

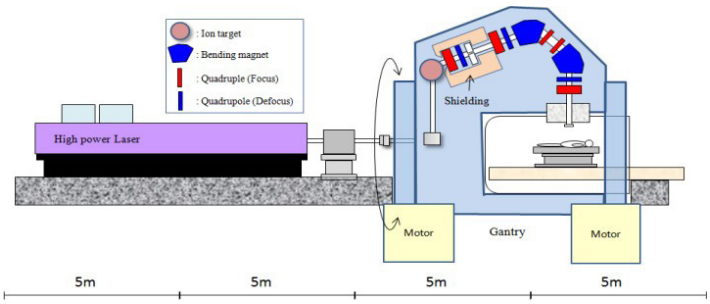

Figure 39: A schematic design showing the laser-driven ion therapy system with a gantry.

Summary

In this paper, the technologies of charged particle accelerators, intended for the therapy of malignant tumors, were briefly presented, without linking them to their life cycle model, a model in the shape of a sigmoid or S-curve, analogous to the life cycle in biology: slow growth at first, followed by accelerating growth that eventually slows down leading to saturation.

These accelerators are the following Betatron and Linac for electrons and photons, synchrocyclotron, isochronous cyclotron and synchrotron for protons, isochronous cyclotron, synchrotron and nonscaling FFAG for providing both types of beams, protons and ions, and from new laser technologies, LWFA for electrons and the TNSA and RPA mechanism for protons and ions.

The energy gain of the charged particles is made by transfer during the repetitive passage through the electric radiofrequency cavities, during the maintenance of the resonance phenomenon.
The product between the electric charge and the speed of light (300 MeV/Tm) acts as a conversion unit from the magnetic rigidity (Bρ) to the relativistic kinetic energy (pc). The magnetic field of the EM force ensures the closed equilibrium orbit and the stability of the betatronic oscillations around it.

The principle of energy gain, i.e. the acceleration of charged particles in vacuum, gases and plasmas, or the transfer of energy from the accelerating electric field to the particles, consists in maintaining the synchronism between the particles and the highfrequency electric fields, until the therapeutic energy is obtained. In the acceleration on a circular trajectory, the energy gain occurs during the equality between the frequency of rotation of the particle and the frequency of the radiofrequency field, in the magnetic field perpendicular to the area of the equilibrium orbit.

The quantity involved in the transport of energy from the beam of ionizing particles (or the radiation field) to the irradiated environment is radiation intensity (or modern - energy fluence rate), in the case of irradiation with photon beams and charged particle fluence in the case of irradiation with charged particles.

When interacting with the environment, the photon beam does not transfer energy. Only charged particles transfer energy. The response of the biological environment, i.e. the energy given to the target organ by the flow of energy when it is irradiated with the photon beam or by the flow of charged particles when they irradiate the target, is represented by the interaction coefficients. They represent the information obtained on the amount of energy of the radiation field imparted to the volume of the tumor.

Technologies for proton therapy are isochronous cyclotrons with sector focus and cyclotrons with spiral focus, which use superconducting magnet technology (B ≤ 10 T). Low cycle synchrotrons (< 3Hz) and fast cycle synchrotrons (> 3 Hz) are also used, which have an equilibrium orbit diameter of (6 – 9) m.

Technologies for heavy ion therapy are represented by heavy ion synchrotrons, which have a production line for proton beams. The diameter of the equilibrium orbit is (18 -25) m, greater than that of protons due to the magnetic rigidity of the particle beam.

New technologies (accelerators) for proton therapy are weakly focused synchrocyclotrons with superconducting magnets (250 MeV, 25 t, r = 0.25 m and B = 9 T). Here we mention both for protons and for heavy ions, the isochronous cyclotron with superconducting magnets (B = 4 T, ρ = 6 m) and the nonscaling FFAG accelerators (B = 3,6 T, ρ = 6.25 m; B = 3.5 T, ρ = 9,2 m). The new technologies (charged particle accelerators) based on laser technology, are LWFA for electrons, TNSA and RPA for protons and ions. Research and development underway to reach the maximum values of 250 MeV for protons and 450 MeV for ions.

References

1. Attix F.H. Introduction to Radiological Physics and Radiation Dosimetry. WILEY-VCH Verlag GmbH & Co.KGaA. 2004.
2. Wiedemann H. Particle Accelerator Physics. Third Edition Springer Verlag Berlin Heidelberg. 2007.
3. Owen H, Lomax A, Jolly S. Current and Future Accelerator Technologies for Charged Particle Therapy. Nuclear Instruments and Methods in Physics Research. 2016.
4. Pedroni E. Center for Proton Radiation Therapy. Paul Scherrer Institute. 2010.
5. Kolomensky A. A, Lebedev A.N. Theory of Cyclic Accelerators. North- Holand Publishing Company Amsterdam. 1966.
6. Sprangle P, Esarey E, Krall J. Laser driven electron accelerationin vacuum, gases, and plasms. Phys Plasmas. 1986; 3.
7. Craddock M. K, Simon K.R. Cyclotrons and Fixed-Field Alternating-Gradient Accelerators. Reviews of Accelerator Science and Technology. 2008.
8. Seltzer S. M. ICRU 85 REPORT No. 85, Fundamental Quantities and Units for Ionizing Radiation. 2011; 11.
9. Scarlat F, Stancu E, Scarisoreanu A. Basic Ionization Dosimetry for Radiological Protection Management. Int J Women's Health Care. 2021; 6: 236-258.
10. Hora H, Laser Plasma Physics: Forces and the nonlinearity principle. 2000.
11. Dorschel B, Schuricht V, Steuer J. The Physics of Radiation Protection. 1995.

12. Scarlat F, Stancu E, Badita E, et al. Ionization dosimetry principles for conventional and laser-driven clinical particle beams. International Journal of Women-s Health Care. 2018; 3: 1-13.
13. IAEA TRS-398. Absorbed Dose Determination in External Beam Radiotherapy: An International Code of Practice for Dosimetry based on Standards of Absorbed Dose to Water. IAEA. 2004.
14. Shapiro J. Radiation Protection. A Guide for Scientists, Regulators and Physicians, fouth edition, Harward University. 2000.
15. Loevinger R, Pfalzner P. M, Eisenlohr H, et al. The IAEA Program in Medical Radiation Dosimetry. Annals New York Academy of Sciences. 1970; 161: 158-167.
16. Quastler H, Adams G.D, Almy G.M, et al. Techniques for Application of the Betatron to Medical Therapy. The American Journal of Roentgenology and Radium Therapy. 1949; 61.
17. Thwaites D.I, Tuohy J. B. Back to the future: the history and development of the clinical linear accelerator. Phys. Med. Biol.2006; 51: R343-R362.
18. Scarlat F, Oproiu C. The 40 MeV Medical Betatron. Experience versus redictions. Proceedings of the EPAC-94, London, England. 1994; 3: 2616.
19. Silari M. Medical Applications of Particle Accelerators University of Freiburg. 2012.
20. Giordanengo S, Donetti M. Dose Delivery Concept and Instrumentation, School Proceedings. 2017; 1: 13-47.
21. Scarlat Florea, Badita E, Stancu E, et al. Basic Principles in conventional and laser driven therapy accelerators. Adv Med Imag and Health Inf. 2019; 1: 1-23.
22. ED Podgorsak. Radiation oncology physics: a handbook for teachers and students. IAEA Vienna. 2005.
23. Garonna A, Amaldi U, Bonomi R, et al. Cyclinac Medical Accelerators Using Pulsed C6+/H2+. EPFL Lausanne. 2010; 7: 1-17.
24. ICRU 83 Journal of the ICRU. 2010.
25. Gregoire V, Mackie TR. Dose prescription, reporting and recording in intensity-modulated radiation therapy: a digest of the ICRU Report 83. Imaging Med. 2011; 3: 367-373.
26. Procedures in External Radiation Therapy Dosimetry with Electron and Photon Beams with Maximum Energies Between 1 and 50 MeV. Acta Radiologica Oncology. 1980; 19: 55-79.
27. ICRU Report 35. Radiation Dosimetry: Electrons with Initial Energies Between 1 and 50 MeV. Bethesda Maryland USA. 1984.
28. Wilson RR. Radiological Use of Fast Protons. Radiology. 1996; 47: 487-491.
29. Verdu-Andres S, Amaldi U, Faus-Golfe A. Literature Review on LINACs and FFAGs for Hadron Therapy. International Journal of Modern Physics. 2011; 10: 1659-1689.
30. Kleeven W, Abs M, Forton E, et al. The IBA Superconducting Synchrocyclotron, Project S2C2. Proceedings of Cyclotrons 2013, Vancouver, BC, Canada. MO4PB02.
31. Smirnov V, Vorozhtsov S. Modern Compact Accelerators of Cyclotron Type for Medical Applications. Physics of Particles and Nuclei. 2016; 47: 863-883.
32. Kostromin SA, Syresin EM. Trends in Accelerator Technology for Hadron Therapy. Physics of Particles and Nuclei Letters. 2013; 10: 833-853.
33. Peggs S, Satogata T, Flanz J. Hadron Therapy Accelerator Technologies. PAC07 25'07.
34. Koji TAKATA. Fundamental Concepts of Particle Accelerators. Accelerator Course Sokendai. JFY. 2010.
35. Weng WT, Mane SR. Fundamentals of Particle Beam Dynamics and Phase Space. BNL 52298. 1991.
36. Kazuo Hiramoto. Synchrotron Technology for Proton Beam Therapy. Educational Workshop. PTCOG 46.
37. Jongen Y. A review of cyclotrons for Hadron Therapy. Cyclotrons 2010 Lanzhou. 2010.
38. Peters A. Particle Therapy using Proton and Ion Beams – From Basic Principles to Daily Operations and Future Concepts. Academic Training Lectures CERN. 2012.
39. Nohtomi A, Sakae T, Tsunashima Y, et al. Dosimetry of pulsed clinical proton beams by a small ionization chamber. Med Phys. 2001; 28: 1431-1435.
40. Schulz-Ertner D, Jäkel O, Schlegel W. Radiation Therapy with Charged Particles. Semin Radiat Oncol. 2006; 16: 249-259.
41. Kanai T, Endo M, Minohara S, et al. Biophysical characteristics of HIMAC clinical irradiation system for heavy-ion radiation therapy. Int J Radiat Oncol Biol Phys. 1999; 44: 201-210.
42. Newhauser WD, Zhang R. The physics of proton therapy. Phys Med Biol. 2015; 60: 155-209.
43. Miller DW. A review of proton beam radiation therapy. Med Phys. 1995; 22: 1943-1654.
44. Schippers JM, Lomax A. Emerging technologies in proton therapy. Acta Oncologica. 2011; 50: 838-850.
45. Flanz J. (The) Future (of) Synchrotrons for Particle Therapy. School Proceedings. 2017.
46. Rossi S. Status of the Hadron Therapy Centers at Heidelberg (HIT) and Pavia (CNAO). 2011.
47. Matsuda K, Itami H, Daishun Chiba, et al. World first Proton Pencil beam Scanning system with FDA Clearance. Hitachi Review. 2009; 58: 225-232.
48. Papash AI, Karamysheva GA, Onischenko LM. Compact Superconducting Synchrocyclotrons at Magnetic Field Level of up to 10 T for Proton and Carbon Therapy. Proceedings of IPAC2011, San Sebastián, Spain. 2011.
49. Galina Karamysheva, Vladimir Aleksandrov, Alim Glazov, et al. IBA C400 Cyclotron Project for hadron therapy. 2007.
50. Sheehy S. FFA Accelerators Fixed Field Alternating Gradient CERN Introductory Accelerator School Constanta Romania. 2018.
51. Yokoi T. Status of PAMELA: An UK Particle Therapy Facility Project Using NS – FFAG. International Journal of Modern Physics. 2011; 26: 1887-1902.

52. Joshi Chandrashekhar, Mori W. The status and evolution of plasma wakefield Particle accelerators. Philosophical transactions Series A Mathematical physical and engineering sciences. 2006; 364: 577-584.
53. Leemans W. Advances in Driven Laser Accelerator R&D.
54. Giulietti A. International School of Physics Enrico Fermi Course CLXXIX "Laser-Plasma Acceleration" Laser-Linac Towards Laser driven Mini-Linac's for biomedical uses Varenna. 2011; 20-25.
55. Schwoerer H, Pfotenhauer S, Jäckel O, et al. Laser-plasma acceleration of quasi-monoenergetic protons from microstructured targets. Nature. 2006; 439: 445-448.
56. Esirkepov T, Borghesi M, Bulanov SV, et al. Highly Efficient Relativistic-Ion Generation in the Laser Piston Regime. Phys Rev Lett. 2004; 92: 175003.
57. Scarlat F, Scarisoreanu A, Verga N, et al. Evaluation of Physical Parameters for Laser-Driven Clinical Hadron Beams. Journal of Intense pulsed Lasers and Applications in Advances Physics. 2014; 4: 55-64.
58. Meer D. Medical Physics Commissioning. School Proceedings. 2017; 1: 285-291.
59. Sakaki H, Hori T, Nishiuchi M, et al. Designing Integrated Laser-Driven Ion Accelerator Systems for Hadron Therapy at PMRC (Photo Medical Research Center), Proceedings of PAC09, Vancouver, BC, Canada TU6PFP009.